Inducible Nitric Oxide Synthase Downmodulates Contact Hypersensitivity by Suppressing Dendritic Cell Migration and Survival

Kazunari Sugita[1], Kenji Kabashima[1,4], Ryutaro Yoshiki[1], Atsuko Ikenouchi-Sugita[2], Masato Tsutsui[3], Jun Nakamura[2], Nobuyuki Yanagihara[3] and Yoshiki Tokura[1]

Nitric oxide (NO) has several important roles in various physiological settings; one of the NO synthases, inducible NO synthase (iNOS), is induced by external stimulation of the skin. A prototypic example of external stimulation is hapten exposure, which induces the T-cell-mediated immune response known as contact hypersensitivity (CHS). We herein report on cutaneous dendritic cell (DC) function in the presence of an iNOS-specific inhibitor during the sensitization phase of CHS. First, we examined epidermal cell (EC) suspensions using flow cytometry with an iNOS antibody and confirmed that iNOS was expressed in the cytoplasm of Langerhans cells (LCs). We then studied the role of iNOS in CHS, and found that responses to DNFB were enhanced by the addition of an iNOS inhibitor during sensitization. Similarly, the iNOS inhibitor augmented FITC-induced migration of cutaneous DCs, including Langerin$^+$ LCs and Langerin$^-$ dermal DCs, to draining lymph nodes. Finally, we showed that iNOS inhibitor enhanced LC survival *in vitro*. We concluded that NO suppresses migration and survival of cutaneous DCs, resulting in a downmodulation of CHS.

Journal of Investigative Dermatology (2010) **130,** 464–471; doi:10.1038/jid.2009.288; published online 3 September 2009

INTRODUCTION

Inducible nitric oxide (NO) synthase (iNOS) is one of the three isoenzymes that generate NO from its precursor L-arginine. In the skin, keratinocytes (Arany *et al.*, 1996), Langerhans cells (LCs) (Qureshi *et al.*, 1996), dermal fibroblasts (Wang *et al.*, 1996), and melanocytes (Rocha and Guillo, 2001) express iNOS upon stimulation with inflammatory cytokines and/or lipopolysaccharide (LPS). Although NO can be proinflammatory when produced in large amounts, it may also regulate adaptive immune responses (Kuchel *et al.*, 2003). The best characterized example is the induction of iNOS by LPS and IFN-γ in murine macrophages (Lu *et al.*, 1996), LCs (Qureshi *et al.*, 1996), and keratinocytes (Yamaoka *et al.*, 2000). Although some information has thus been accumulated regarding the *in vitro* effects of iNOS on skin immunocompetent cells, the *in vivo* actions of iNOS remain unknown.

Murine contact hypersensitivity (CHS) is an antigen-specific immune response consisting of the two phases, namely, sensitization and elicitation. The constituents involved in its pathogenesis are Th1/Tc1 cells serving as helper/effector cells (Akiba *et al.*, 2002); cutaneous dendritic cells (DCs), including epidermal LCs and dermal DCs (dDCs), as antigen-presenting cells (Kissenpfennig and Malissen, 2006); and keratinocytes as a source of IL-1α, tumor necrosis factor-α, and GM-CSF to the LCs (Sugita *et al.*, 2007). iNOS is induced in LCs and keratinocytes by contact allergens; this supports the view that iNOS has a role in CHS (Morita *et al.*, 1996). It has previously been reported that an iNOS inhibitor injected intradermally during the elicitation phase suppressed CHS responses (Ross *et al.*, 1998), but the specificity of this iNOS inhibitor is not clear; furthermore, the role of iNOS in the sensitization phase remains unknown.

In this study, we investigated the effects of an iNOS-specific inhibitor in order to determine whether iNOS functions as a positive or negative regulator in CHS. Our results show that iNOS suppresses the CHS response by downmodulating the migration and survival of DCs.

RESULTS

iNOS inhibitor enhances CHS response to DNFB

First, we tested the degree of CHS response in mice treated with L-N^6-iminoethyl-lysine (L-NIL), an iNOS inhibitor.

[1]*Department of Dermatology, University of Occupational and Environmental Health, Kitakyushu, Japan;* [2]*Department of Psychiatry, University of Occupational and Environmental Health, Kitakyushu, Japan;* [3]*Department of Pharmacology, University of Occupational and Environmental Health, Kitakyushu, Japan and* [4]*Department of Dermatology, Kyoto University Graduate School of Medicine, Kyoto, Japan*

Correspondence: Dr K Sugita, Department of Dermatology, University of Occupational and Environmental Health, 1-1 Iseigaoka, Yahatanishi-ku, Kitakyushu 807-8555, Japan. E-mail: k-sugita@med.uoeh-u.ac.jp

Abbreviations: Ab, antibody; B6, C57BL/6; CCL21, CC chemokine ligand 21; CCR7, CC chemokine receptor 7; CHS, contact hypersensitivity; DC, dendritic cell; dDC, dermal DC; EC, epidermal cell; iNOS, inducible nitric oxide synthase; LC, Langerhans cell; L-NIL, L-N^6-iminoethyl-lysine; LPS, lipopolysaccharide; NO, nitric oxide; PBS, phosphate-buffered saline

Received 2 March 2009; revised 9 July 2009; accepted 19 July 2009; published online 3 September 2009

The mice were sensitized and challenged with DNFB, and their ear swelling responses were measured 24 hours after the challenge. A significantly higher degree of ear swelling response was observed in C57BL/6 (B6) mice treated intraperitoneally with L-NIL throughout the sensitization phase than in non-treated control mice (Figure 1a). Similar results were obtained 48 hours after the challenge (data not shown). In addition, histological analysis of the L-NIL-treated mice showed a remarkable infiltration of lymphocytes into the edematous dermis, which was not seen in untreated mice (Figure 1b). To confirm that L-NIL was biologically active in the skin when administered systemically, we measured the NOx ($NO_2^- + NO_3^-$) concentration of DNFB-sensitized skin. NOx production induced by DNFB was inhibited by an intraperitoneal injection of L-NIL (Supplementary Figure S1), suggesting that L-NIL is biologically active in lesional skin even when it is administered systemically.

iNOS expression in keratinocytes and LCs

Freshly isolated murine epidermal cells (ECs) were incubated for 24 hours in a culture medium, and the LCs and keratinocytes among them were analyzed for iNOS expression with flow cytometry. Both the keratinocytes and the LCs bore iNOS in the cytoplasm (Figure 2a). iNOS expression was greater in the mature LCs (major histocompatibility complex (MHC) class II high expression) than in the immature LCs (MHC class II intermediate expression). We carried out the same analysis on ECs that had been cultured for 24 hours in the presence of LPS, and found that LPS increased the number of LCs that highly expressed iNOS (Figure 2b).

iNOS inhibitor increases cutaneous DC accumulation in regional lymph nodes

To investigate the *in vivo* significance of iNOS for cutaneous DCs, we performed an FITC-induced cutaneous

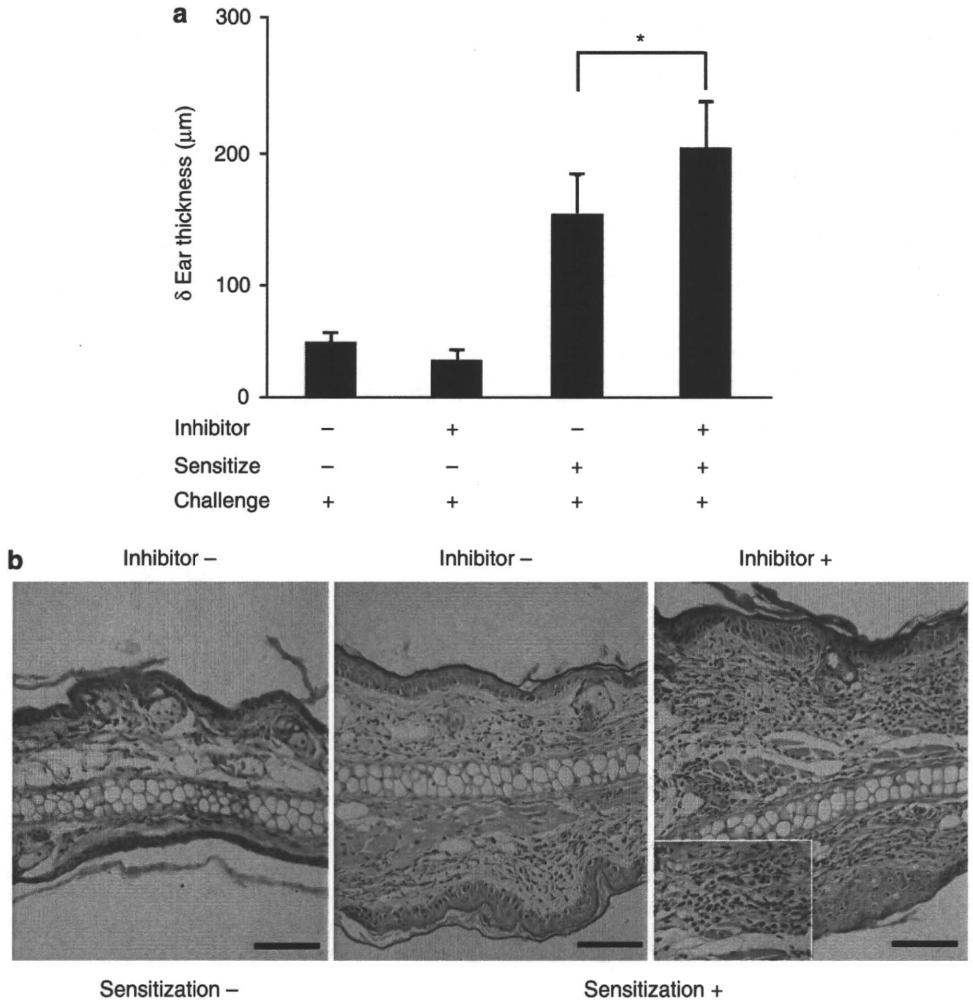

Figure 1. Increased CHS response to DNFB caused by blockade of iNOS. (**a**) For CHS model, B6 mice were immunized by the application of 0.5% DNFB to their shaved abdomens. They were challenged on both ears with 0.3% DNFB. iNOS inhibitor was applied through intraperitoneal injection (2.5 mg in 0.5 ml PBS twice daily). Ear thickness swelling was measured 24 hours later. Data are expressed as the mean ± SD of five mice. *$P<0.05$. (**b**) Non-sensitized ears, challenged ears, and challenged ears from non-treated mice (inhibitor –) were stained with hematoxylin and eosin. Inset: close-up view of hematoxylin and eosin staining of ears from mice treated with iNOS inhibitor, showing perivascular lymphocytic infiltration. Bar = 80 μm. Data are from three independent experiments.

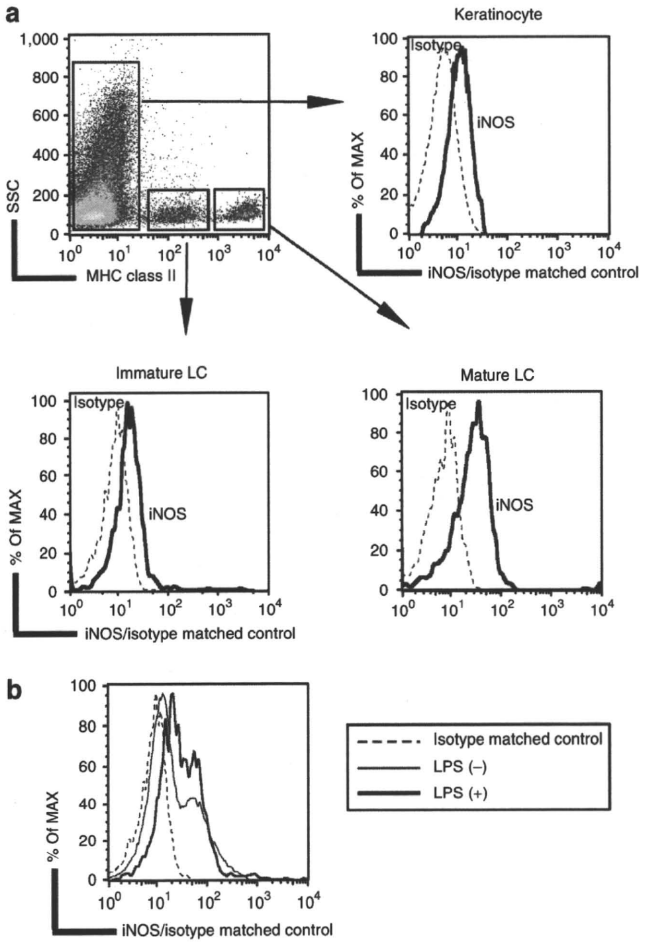

Figure 2. Expression of iNOS by both keratinocytes and LCs. (**a**) EC suspensions were analyzed for the expression of iNOS by means of flow cytometry. For intracellular detection of iNOS, cell fixation–permeabilization was performed before immunolabeling with anti-iNOS and anti-MHC class II mAbs. LCs or keratinocytes were gated by MHC class II positivity. (**b**) EC suspensions from naive mice were cultured with or without LPS (1 μg ml^{-1}) for 24 hours. The cultured cells were subjected to a flow cytometric analysis, which allowed us to measure the expression of iNOS. Data are from three independent experiments.

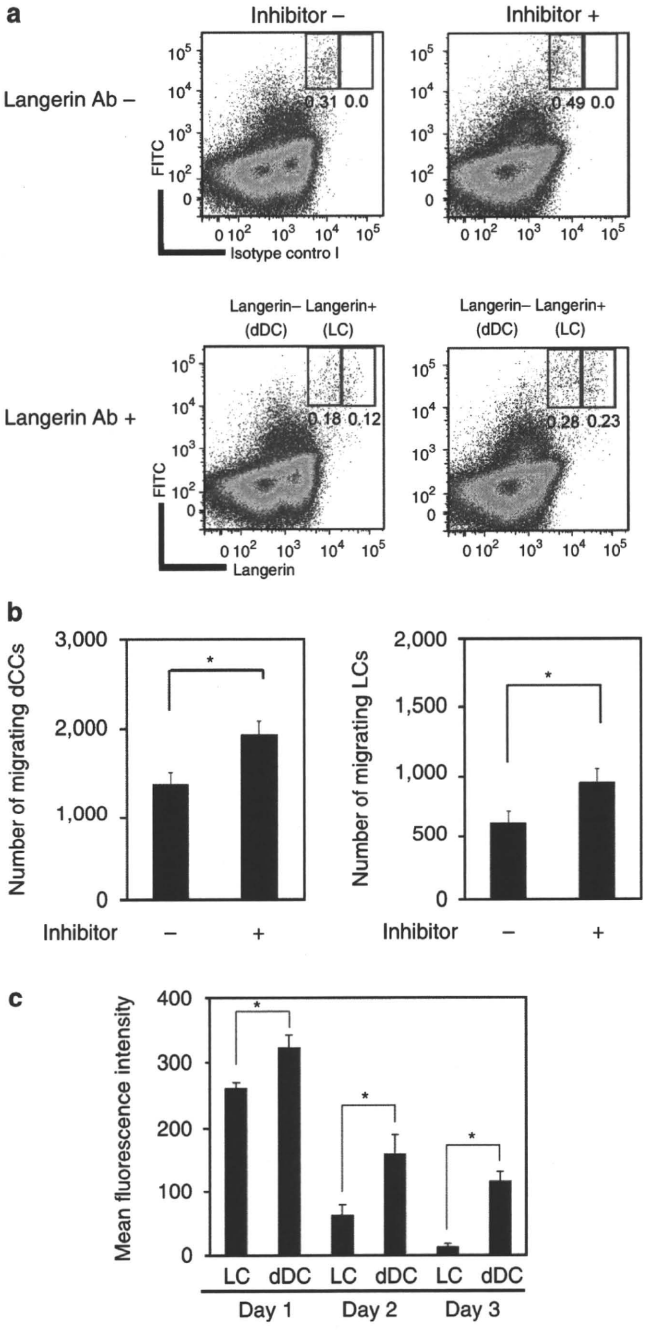

Figure 3. Augmented cutaneous DC accumulation in regional lymph nodes by iNOS blockade. (**a**) Langerin expression and FITC fluorescence in cells derived from regional lymph nodes were analyzed by means of flow cytometry 72 hours after the application of 200 μl of 2% FITC. The percentage of migrating LCs is indicated. (**b**) Migrating dDCs or LCs were counted 72 hours after FITC painting. Columns show the mean ± SD from at least four mice per group. *$P<0.05$. (**c**) Expression of iNOS in migrating LCs and dDCs. Draining lymph node cells were taken from mice painted with FITC on the abdomen and stained with anti-MHC class II, Langerin, and iNOS mAbs. Days 1, 2, and 3 indicate the number of days since FITC painting. Data are expressed as mean fluorescence intensity (MFI) for iNOS. MFI was the value of LCs or dDCs subtracted from that of the isotype-matched control. Columns show the mean ± SD. *$P<0.01$. Results are representative of three independent experiments.

DC migration assay. FITC applied to the skin is taken up by cutaneous DCs, which subsequently migrate to the draining lymph nodes as FITC$^+$ MHC class II$^+$ cells. We intraperitoneally injected L-NIL, an iNOS inhibitor (2.5 mg in 0.5 ml phosphate-buffered saline (PBS) twice daily for 4 consecutive days) or the equivalent amount of PBS into mice; 24 hours after the last injection, we applied FITC to the abdomen. We then isolated axillary and inguinal draining lymph node cells 72 hours after FITC application and characterized the FITC$^+$MHC class II$^+$ cutaneous DCs therein by flow cytometry. Staining for Langerin showed that two subsets of the FITC$^+$ MHC class II$^+$ cutaneous DCs, the dDCs and LCs, were present in significantly greater numbers because of treatment with iNOS inhibitor (Figure 3a and b). Therefore, the blockade of iNOS promoted lymph node accumulation of cutaneous DCs in response to skin exposure to an antigen.

iNOS expression in migrating LCs and dDCs

We examined iNOS expression in freshly isolated LCs and dDCs, both of which are capable of migrating into the lymph nodes on sensitization. The expression of iNOS in these cells was examined with FITC and anti-Langerin mAb. FITC was applied to the abdomen, and draining lymph node cells were sampled 24, 48, and 72 hours later. These cells were then labeled with anti-MHC class II mAb, anti-Langerin Ab, and anti-iNOS Ab. Although LCs are positive for Langerin, most dermal DCs are negative for Langerin (Nagao *et al.*, 2009), iNOS was present in both LCs and dDCs. The mean fluorescence intensity for iNOS was as follows: LC, 11.9 ± 4.1; dDC, 36.6 ± 20.5 (mean ± SD of three mice). These data suggested that iNOS was weakly expressed only in freshly isolated LCs and dDCs, in amounts too small to be statistically significant. Nevertheless, we were able to observe that the dDCs showed a higher mean fluorescence intensity of iNOS expression than the LCs did (Figure 3c).

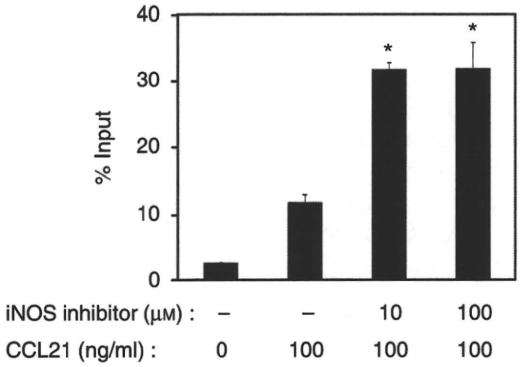

Figure 4. Chemotactic activity of epidermal LCs to CCL21. EC suspensions were incubated with or without iNOS inhibitor plus LPS in culture medium for 9 hours and applied to a transwell. CCL21 at 100 ng ml^{-1} was administered to the lower chamber. Migrating epidermal LCs in the lower chamber were identified as belonging to the MHC class II$^+$ subset. The number of migrating LCs was calculated. Columns represent the mean ± SD of triplicated transwells, and data are from three independent experiments. *$P<0.01$.

Chemotactic activity of LCs to CCL21

EC suspensions were incubated with LPS in a culture medium for 9 hours and applied to transwells in the presence or absence of L-NIL, an iNOS inhibitor. The migrating LCs in the lower chamber were identified as MHC class II$^+$ cells. CCL21 (CC chemokine ligand 21), a cytokine expressed in secondary lymphoid organs that mediates the chemotaxis of lymphocytes and DCs through its receptor, CCR7 (CC chemokine receptor 7; Saeki *et al.*, 1999), was then added to the lower chamber. All LCs exhibited a strong chemotactic response to this chemokine, but this response was significantly increased by the iNOS inhibitor (Figure 4).

iNOS inhibitor caused no alteration of the expression of co-stimulatory molecules or CCR7

The chemotaxis-promoting activity of the iNOS inhibitor, described above, raised the possibility that the iNOS inhibitor upregulates the expression of co-stimulatory molecules and CCR7. To determine whether this is the case, freshly isolated ECs were cultured for 24 hours in the presence or absence of the iNOS inhibitor, and the expression levels of these molecules were monitored by gating for MHC class II$^+$ LCs. After 24 hours of culture, a single population of LCs usually divides into two populations, with different expression levels of co-stimulatory molecules and CCR7 (Sugita *et al.*, 2007) (Figure 5a). The addition of the iNOS inhibitor did not alter the expression of CD86, CD80, CD40, or CCR7 (Figure 5a and b). In chemotaxis, however, the expression of

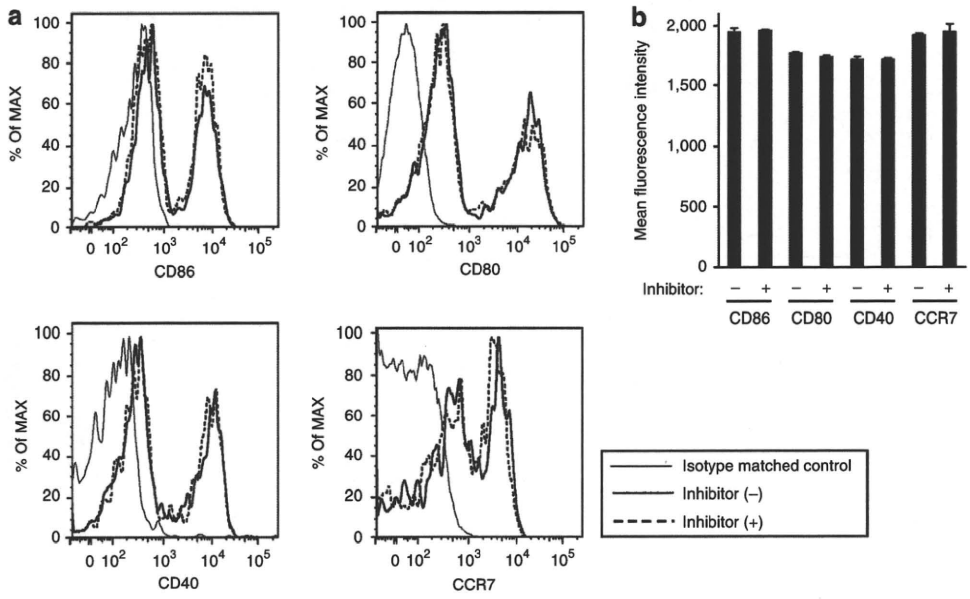

Figure 5. No modulation of CD86, CD80, CD40, or CCR7 expression in LCs by iNOS inhibitor. (**a** and **b**) EC suspensions from naive mice were cultured for 24 hours with or without iNOS inhibitor. The cultured LCs were examined for their expression levels of CD86, CD80, CD40, and CCR7. Data are representative of three independent experiments.

CCR7 in DCs is not sufficient to guarantee its functionality (Sanchez-Sanchez *et al.*, 2006); therefore, it is possible that iNOS alters certain downstream functions of LCs without affecting CCR7 expression.

iNOS inhibitor reduces LPS-induced apoptosis of LC

We then evaluated the effect of endogenous iNOS activity on the viability of LCs. EC suspensions from the earlobes of B6 mice were cultured for 9 hours with or without LPS in the presence or absence of L-NIL, an iNOS inhibitor. LPS stimulation reduced the number of LCs, but this reduction was reversed by the addition of the iNOS inhibitor (Figure 6a). It has been reported that epidermal LCs are unable to proliferate *in vitro* when they are incubated as an EC suspension (Schuler and Steinman, 1985), suggesting that the observed effects of the iNOS inhibitor stem from a survival change.

To examine whether the iNOS inhibitor promotes the survival of LCs, cellular viability was assessed through flow cytometry after Annexin V/propidium iodide staining and 9 hours of culture (Figure 6b). This flow cytometry experiment used anti-MHC class II and anti-CD11c mAbs. The percentage of Annexin V and propidium iodide double-positive cells in samples that had been treated with 100 μM iNOS inhibitor and those that had not was as follows: 100 μM, 1.6 ± 0.4%; no addition, 2.2 ± 1.0% (mean ± SD, $n = 3$). These results suggest that the reduction of apoptotic cells that occurs through iNOS inhibitor treatment is not due to the increment of necrotic cells. We found that LPS-induced apoptosis of LCs was reduced by the addition of the iNOS inhibitor (Figure 6c), suggesting that the iNOS inhibitor promotes DC survival.

DISCUSSION

The results of this study on the effects of an iNOS inhibitor include several major findings about the involvement of NO in the sensitization phase of CHS. First, CHS as a model of acquired skin immune response was enhanced by treatment with the iNOS inhibitor. Second, the iNOS inhibitor markedly increased the number of migrating cutaneous DCs. Accordingly, the chemotactic response of LCs to CCL21 was enhanced by *in vitro* incubation with the iNOS inhibitor. Finally, the iNOS inhibitor was capable of reducing LPS-induced apoptosis of LCs.

It has generally been believed that iNOS is involved in CHS as a producer of NO and a trigger of inflammatory responses (Cals-Grierson and Ormerod, 2004). It has been

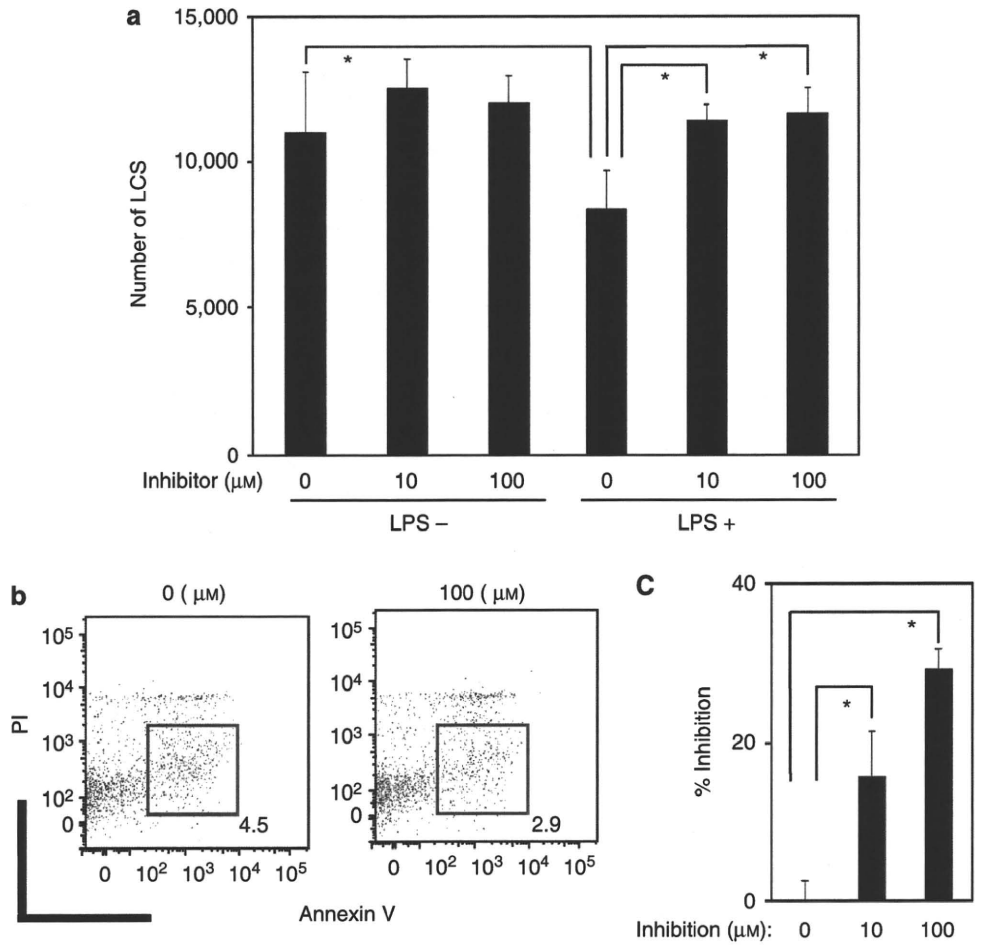

Figure 6. The effect of LPS on LC survival. (**a**) EC suspensions were cultured with or without LPS and iNOS inhibitor for 9–12 hours. iNOS inhibitor dose dependently increased the number of LCs. Columns show the mean ± SD. *$P<0.05$. Data are representative of three independent experiments. (**b**) Apoptosis was determined using annexin V/propidium iodide double staining. (**c**) The percentage inhibition is calculated. Data represent the mean ± SD. *$P<0.05$.

reported that iNOS and NO were produced in human skin subjected to positive patch tests to contact allergens (Cruz *et al.*, 2007; Ormerod *et al.*, 1997) and to the irritant sodium lauryl sulfate; nevertheless, it remains controversial whether iNOS is inhibitory or augmentative in CHS (Ross and Reske-Kunz, 2001). It has also been reported that an iNOS inhibitor exerted a suppressive effect on the CHS response to 2,4,6-trinitrochlorobenzene (TNCB) (Musoh *et al.*, 1998), although this effect was limited to the first few hours of the response, and neither NO production, NO-expressing cells, nor NOS isoenzymes were identified. Thus, the mode of action of iNOS in CHS remains a matter of debate.

It is possible that iNOS first modulates keratinocytes so that they produce cytokines, thereby subsequently modifying LC function. Yet, we found that the production levels of GM-CSF and tumor necrosis factor-α in the culture supernatant of primary keratinocytes of B6 mice cultured for 72 hours were not significantly affected by the presence of the iNOS inhibitor (Supplementary Figure S2). With regard to the effect of iNOS on T cells, we cultured immune $CD4^+$ T cells for 72 hours with varying concentrations of the iNOS inhibitor in the presence of anti-CD3 mAb and found that the iNOS inhibitor was incapable of stimulating T cells *per se* (Supplementary Figure S3).

LCs have traditionally been believed to have a role in the induction of CHS, but three research groups have reported three contradictory findings after applying haptens to transgenic mice deficient in LCs: a diminished reaction (Bennett *et al.*, 2005), an enhanced reaction (Kaplan *et al.*, 2005), and an unchanged response (Kissenpfennig *et al.*, 2005). Moreover, recent findings suggest that dDCs has a critical role in initiating CHS (Fukunaga *et al.*, 2008). In our study, dDCs augmented iNOS expression in response to hapten application more than LCs did. Our findings suggest that iNOS can suppress cutaneous DC migration and survival. Given that, in CHS, dDCs and LCs have positive and regulatory capacities, respectively, our findings on cutaneous DCs seem to be consistent with the observation that iNOS inhibitor induces an enhancement of CHS.

The findings of our study are clinically relevant in two respects. First, iNOS and NO exert immunosuppressive effects on cutaneous inflammation. In this context, the *in vivo* immunosuppressive effect of NO has also been shown in human studies (Kuchel *et al.*, 2003). Second, iNOS reduces cutaneous DC function and survival in the sensitization phase of CHS. The observation that NO directly reduces the number of LCs in the human epidermis supports our conclusion (Mowbray *et al.*, 2008).

MATERIALS AND METHODS

Animals and reagents

Female B6 mice were purchased from Japan SLC (Hamamatsu, Japan). All experiments were conducted on 8-week-old mice. The mice were maintained on a 12-hour light/dark cycle under a specific pathogen-free condition. All protocols were approved by the Institutional Animal Care and Use Committee of the University of Occupational and Environmental Health. L-NIL (a highly selective inhibitor of iNOS enzymatic activity) and LPS were obtained from Sigma-Aldrich (St Louis, MO). CCL21 was purchased from R&D Systems (Minneapolis, MN).

DNFB-induced CHS model

B6 mice were sensitized through the application of 25 μl of 0.5% (v/v) DNFB in 4:1 acetone/olive oil to their shaved abdomens on day 0. They were then challenged on both sides of each ear with 20 μl of 0.3% (v/v) DNFB. Ear thickness change was calculated as follows: (ear thickness 24 or 48 hours after challenge)−(ear thickness before challenge). iNOS was inhibited with L-NIL as described previously (Diefenbach *et al.*, 1998). Briefly, L-NIL was applied by intraperitoneal injection (2.5 mg in 0.5 ml PBS twice daily) for 6 consecutive days starting 1 day before sensitization. We chose his protocol because treatment with L-NIL at this concentration and frequency for 4-13 days is one of the most common methods of blocking *in vivo* activity of iNOS (Diefenbach *et al.*, 1998; Stallmeyer *et al.*, 1999).

EC preparation and culture

EC suspensions were prepared as described previously (Tokura *et al.*, 1994). Ears of naive mice were split along the plane of the cartilage, which was then removed together with the subcutaneous tissue. These specimens were incubated for 1 hour at 37 °C in a 0.2% solution of trypsin in PBS. After incubation, the epidermis was separated from the dermis and the separated epidermal sheets were rubbed to disperse the ECs in PBS supplemented with 10% fetal calf serum. The cells were filtered and washed twice in PBS. As a culture medium, RPMI-1640 (Sigma-Aldrich) was supplemented with 10% heat-inactivated fetal calf serum, 5×10^{-5} M 2-mercaptoethanol, 2 mM L-glutamine, 25 mM HEPES (4-(2-hydroxyethyl)-1-piperazineethanesulfonic acid), 1 mM nonessential amino acids, 1 mM sodium pyruvate, 100 U ml^{-1} penicillin, and 100 μg ml^{-1} streptomycin.

Preparation of dermal cell suspensions

Dermal cells were obtained from normal murine skin from which the epidermis had been removed. Samples were minced and incubated for 2 hours at 37 °C in RPMI-1640 medium (Invitrogen, Carlsbad, CA) supplemented with collagenase (2 mg ml^{-1}; Sigma-Aldrich), hyaluronidase (260 U ml^{-1}; Sigma-Aldrich), DNase (0.1 mg ml^{-1}; ICN, Costa Mesa, CA), and 10 mM HEPES (Sigma-Aldrich). The obtained cells were filtered through a 40-μm filter.

Flow cytometry

For flow cytometry, cells were plated at a density of 1×10^6 cells per well in 96-well U-bottomed plates (Falcon, BD Biosciences, San Jose, CA). Cells were then stained for 20 minutes on ice with mAbs in 25 μl of PBS containing 2% fetal calf serum, 1 mM EDTA, and 0.1% NaN_3, and washed twice with 200 μl of this buffer. Data were collected on a FACSCanto system (BD Biosciences) and analyzed with FlowJo software (TreeStar, San Carlos, CA). The mAbs used were as follows: FITC-conjugated anti-CD86 and Annexin V mAbs, PE-conjugated anti-CD80 and CD40 mAbs, PE-Cy5-conjugated anti-MHC class II mAb, APC-conjugated anti-CD11c mAb (all from BD Biosciences), and PE-Cy7-conjugated anti-CCR7 mAb (eBioscience, San Diego, CA). For detection of Langerin and iNOS, anti-Langerin Ab (eBioscience), PE-conjugated anti-iNOS Ab (Santa Cruz Biotechnology, Santa Cruz, CA), and PE-Cy5-conjugated streptavidin were

used after fixation and permeabilization of cells using a Cytofix/Cytoperm Kit (BD Biosciences).

Histology

At 48 hours after the challenge with hapten, the ears of B6 mice were excised and fixed in 10% formaldehyde. Sections of 5-μm thickness were prepared and stained with hematoxylin and eosin.

FITC-induced cutaneous DC migration

The shaved abdomens of the mice were painted with 200 μl of 2% FITC (Sigma-Aldrich) dissolved in a 1:1 (v/v) acetone/dibutyl phthalate (Sigma-Aldrich) mixture, and the iNOS inhibitor was applied through intraperitoneal injection (2.5 mg in 0.5 ml PBS) twice daily for 4 days. Cutaneous DCs migrating into the draining inguinal and axillary lymph nodes were then counted by means of flow cytometry (Kabashima *et al.*, 2007) using Flow-Count Fluorospheres (Beckman Coulter, Fullerton, CA). The principle of Flow-Count Fluorospheres is based on the precise mixing of microparticles whose concentration and volume are known. Before flow cytometric analysis, 10 μl of Flow-Count Fluorospheres were added to each specimen. The percentages of fluorospheres and migrating DCs within each node were then determined using the FACSCanto system (BD Biosciences). To find the number of migrating DCs, the ratio of DCs to fluorospheres was counted using the following formula, based on Reimann *et al.* (2000), with some modifications: number of migrating DCs = (percentage of migrating DCs/percentage of fluorospheres) × number of fluorospheres.

Chemotaxis assay

EC suspensions were incubated for 9 hours with or without the iNOS inhibitor, and then tested for transmigration across uncoated 5-μm transwell filters (Corning Costar, Corning, NY) to CCL21 or medium in the lower chamber for 3 hours. Migrating cells were enumerated by means of flow cytometry (Ngo *et al.*, 1998). The medium used in this assay was RPMI-1640 with 0.5% fatty acid-free bovine serum albumin (Calbiochem, San Diego, CA).

Apoptosis analysis

The EC suspensions from B6 mice were stained with PE-Cy5-conjugated anti-MHC class II mAb for 20 minutes on ice, then stained with FITC-conjugated Annexin V and propidium iodide (BD Pharmingen, Franklin Lakes, NJ), according to the manufacturer's protocol. The number of LCs was assessed by means of flow cytometry with anti-MHC class II and APC-conjugated anti-CD11c mAbs. Apoptosis in LCs was analyzed using a FACSCanto system with FlowJo software.

Statistical analysis

Data were analyzed using an unpaired two-tailed *t*-test. $P<0.05$ was considered to be significant.

CONFLICT OF INTEREST

The authors state no conflict of interest.

ACKNOWLEDGMENTS

This work was supported in part by a Grant-in-Aid for Scientific Research from the Ministry of Education, Culture, Sports, Science, and Technology of Japan, the Ministry of Health, Labor, and Welfare of Japan, and by a Grant from Shiseido Co. Ltd.

SUPPLEMENTARY MATERIAL

Supplementary material is linked to the online version of the paper at http://www.nature.com/jid

REFERENCES

Akiba H, Kehren J, Ducluzeau MT, Krasteva M, Horand F, Kaiserlian D *et al.* (2002) Skin inflammation during contact hypersensitivity is mediated by early recruitment of CD8+ T cytotoxic 1 cells inducing keratinocyte apoptosis. *J Immunol* 168:3079–87

Arany I, Brysk MM, Brysk H, Tyring SK (1996) Regulation of inducible nitric oxide synthase mRNA levels by differentiation and cytokines in human keratinocytes. *Biochem Biophys Res Commun* 220:618–22

Bennett CL, van Rijn E, Jung S, Inaba K, Steinman RM, Kapsenberg ML *et al.* (2005) Inducible ablation of mouse Langerhans cells diminishes but fails to abrogate contact hypersensitivity. *J Cell Biol* 169:569–76

Cals-Grierson MM, Ormerod AD (2004) Nitric oxide function in the skin. *Nitric Oxide* 10:179–93

Cruz MT, Neves BM, Goncalo M, Figueiredo A, Duarte CB, Lopes MC (2007) Effect of skin sensitizers on inducible nitric oxide synthase expression and nitric oxide production in skin dendritic cells: role of different immunosuppressive drugs. *Immunopharmacol Immunotoxicol* 29:225–41

Diefenbach A, Schindler H, Donhauser N, Lorenz E, Laskay T, MacMicking J *et al.* (1998) Type 1 interferon (IFNalpha/beta) and type 2 nitric oxide synthase regulate the innate immune response to a protozoan parasite. *Immunity* 8:77–87

Fukunaga A, Khaskhely NM, Sreevidya CS, Byrne SN, Ullrich SE (2008) Dermal dendritic cells, and not Langerhans cells, play an essential role in inducing an immune response. *J Immunol* 180:3057–64

Kabashima K, Shiraishi N, Sugita K, Mori T, Onoue A, Kobayashi M *et al.* (2007) CXCL12–CXCR4 engagement is required for migration of cutaneous dendritic cells. *Am J Pathol* 171:1249–57

Kaplan DH, Jenison MC, Saeland S, Shlomchik WD, Shlomchik MJ (2005) Epidermal Langerhans cell-deficient mice develop enhanced contact hypersensitivity. *Immunity* 23:611–20

Kissenpfennig A, Henri S, Dubois B, Laplace-Builhe C, Perrin P, Romani N *et al.* (2005) Dynamics and function of Langerhans cells *in vivo*: dermal dendritic cells colonize lymph node areas distinct from slower migrating Langerhans cells. *Immunity* 22:643–54

Kissenpfennig A, Malissen B (2006) Langerhans cells—revisiting the paradigm using genetically engineered mice. *Trends Immunol* 27:132–9

Kuchel JM, Barnetson RS, Halliday GM (2003) Nitric oxide appears to be a mediator of solar-simulated ultraviolet radiation-induced immunosuppression in humans. *J Invest Dermatol* 121:587–93

Lu L, Bonham CA, Chambers FG, Watkins SC, Hoffman RA, Simmons RL *et al.* (1996) Induction of nitric oxide synthase in mouse dendritic cells by IFN-gamma, endotoxin, and interaction with allogeneic T cells: nitric oxide production is associated with dendritic cell apoptosis. *J Immunol* 157:3577–86

Morita H, Hori M, Kitano Y (1996) Modulation of picryl chloride-induced contact hypersensitivity reaction in mice by nitric oxide. *J Invest Dermatol* 107:549–52

Mowbray M, Tan X, Wheatley PS, Rossi AG, Morris RE, Weller RB (2008) Topically applied nitric oxide induces T-lymphocyte infiltration in human skin, but minimal inflammation. *J Invest Dermatol* 128: 352–60

Musoh K, Nakamura N, Ueda Y, Inagaki N, Nagai H (1998) Possible role of nitric oxide in IgE-mediated allergic cutaneous reaction in mice. *Int Arch Allergy Immunol* 115:91–6

Nagao K, Ginhoux F, Leitner WW, Motegi SI, Bennett CL, Clausen BE *et al.* (2009) Murine epidermal Langerhans cells and langerin-expressing dermal dendritic cells are unrelated and exhibit distinct functions. *Proc Natl Acad Sci USA* 106:3312–7

Ngo VN, Tang HL, Cyster JG (1998) Epstein–Barr virus-induced molecule 1 ligand chemokine is expressed by dendritic cells in lymphoid tissues and strongly attracts naive T cells and activated B cells. *J Exp Med* 188:181–91

Ormerod AD, Dwyer CM, Reid A, Copeland P, Thompson WD (1997) Inducible nitric oxide synthase demonstrated in allergic and irritant contact dermatitis. *Acta Derm Venereol* 77:436–40

Qureshi AA, Hosoi J, Xu S, Takashima A, Granstein RD, Lerner EA (1996) Langerhans cells express inducible nitric oxide synthase and produce nitric oxide. *J Invest Dermatol* 107:815–21

Reimann KA, O'Gorman MR, Spritzler J, Wilkening CL, Sabath DE, Helm K *et al.* (2000) Multisite comparison of CD4 and CD8 T-lymphocyte counting by single- versus multiple-platform methodologies: evaluation of Beckman Coulter flow-count fluorospheres and the tetraONE system. The NIAID DAIDS New Technologies Evaluation Group. *Clin Diagn Lab Immunol* 7:344–51

Rocha IM, Guillo LA (2001) Lipopolysaccharide and cytokines induce nitric oxide synthase and produce nitric oxide in cultured normal human melanocytes. *Arch Dermatol Res* 293:245–8

Ross R, Gillitzer C, Kleinz R, Schwing J, Kleinert H, Forstermann U *et al.* (1998) Involvement of NO in contact hypersensitivity. *Int Immunol* 10:61–9

Ross R, Reske-Kunz AB (2001) The role of NO in contact hypersensitivity. *Int Immunopharmacol* 1:1469–78

Saeki H, Moore AM, Brown MJ, Hwang ST (1999) Cutting edge: secondary lymphoid-tissue chemokine (SLC) and CC chemokine receptor 7 (CCR7) participate in the emigration pathway of mature dendritic cells from the skin to regional lymph nodes. *J Immunol* 162:2472–5

Sanchez-Sanchez N, Riol-Blanco L, Rodriguez-Fernandez JL (2006) The multiple personalities of the chemokine receptor CCR7 in dendritic cells. *J Immunol* 176:5153–9

Schuler G, Steinman RM (1985) Murine epidermal Langerhans cells mature into potent immunostimulatory dendritic cells *in vitro*. *J Exp Med* 161:526–46

Stallmeyer B, Kampfer H, Kolb N, Pfeilschifter J, Frank S (1999) The function of nitric oxide in wound repair: inhibition of inducible nitric oxide-synthase severely impairs wound reepithelialization. *J Invest Dermatol* 113:1090–8

Sugita K, Kabashima K, Atarashi K, Shimauchi T, Kobayashi M, Tokura Y (2007) Innate immunity mediated by epidermal keratinocytes promotes acquired immunity involving Langerhans cells and T cells in the skin. *Clin Exp Immunol* 147:176–83

Tokura Y, Yagi J, O'Malley M, Lewis JM, Takigawa M, Edelson RL *et al.* (1994) Superantigenic staphylococcal exotoxins induce T-cell proliferation in the presence of Langerhans cells or class II-bearing keratinocytes and stimulate keratinocytes to produce T-cell-activating cytokines. *J Invest Dermatol* 102:31–8

Wang R, Ghahary A, Shen YJ, Scott PG, Tredget EE (1996) Human dermal fibroblasts produce nitric oxide and express both constitutive and inducible nitric oxide synthase isoforms. *J Invest Dermatol* 106:419–27

Yamaoka J, Kume T, Akaike A, Miyachi Y (2000) Suppressive effect of zinc ion on iNOS expression induced by interferon-gamma or tumor necrosis factor-alpha in murine keratinocytes. *J Dermatol Sci* 23:27–35

Cholinergic Urticaria: Studies on the Muscarinic Cholinergic Receptor M3 in the Anhidrotic and Hypohidrotic Skin

Journal of Investigative Dermatology (2010) **0,** 000–000. doi:10.1038/jid.2010.188

TO THE EDITOR

Cholinergic urticaria (CU) is a sweating-associated, syringeal orifice-coincident wheal mediated by acetylcholine. CU is occasionally associated with depressed sweating, as reported under the name of anhidrosis (complete lack of sweating) or hypohidrosis (incomplete lack of sweating) (Itakura *et al.*, 2000). There have been reported 29 patients with CU with anhidrosis and/or hypohidrosis (CUAH) (Kay and Maibach, 1969; Itakura *et al.*, 2000; Yoshida *et al.*, 2009). One hypothesis for the relationship between the wheal formation and the depressed sweating is that the patients are hypersensitive to unknown substance(s) in their sweat and develop wheals in response to sweat leaking from the syringeal ducts to the dermis possibly by obstruction of the ducts (Adachi *et al.*, 1994; Kobayashi *et al.*, 2002). In fact, some patients with common CU exhibit wheals to intradermal injection of the patients' own diluted sweat as well as acetylcholine and histologically show sweat duct obstruction (Fukunaga *et al.*, 2005). However, none of the reported patients with CUAH were positive to the intradermally injected autologous sweat, suggesting that "sweat hypersensitivity" is not responsible for CUAH. In addition, if sweat hypersensitivity is the mechanism, the anhidrotic area should be the predilection site for wheal, but such an observation has not been reported.

The study design was approved by the review board of University of Occupational and Environmental Health. Measurements in this study were performed after informed consent had been obtained. The study was conducted according to the Declaration of Helsinki guidelines. To address its mechanism, we investigated four nonsmoker male CUAH patients, aged 23 (case 1), 24 (case 2), 50 (case 3), and 36 years (case 4). The exercise challenge and iodine–starch assessment for sweat induction (Kobayashi *et al.*, 2002) revealed that the skin surfaces of all patients were divided into the anhidrotic and hypohidrotic areas (Figure 1a). The skin with normal sweating was not seen in any patient. As represented by case 1, the applied iodine–starch was discolored by sweat in the hypohidrotic but not anhidrotic area (Figure 1b, left), and following exercise challenge, the patients developed pinpoint wheals in only the hypohidrotic areas (Figure 1b, right). Intradermal injection of acetylcholine yielded wheal with sweating at only the hypohidrotic areas (Figure 1c). The injection of autologous sweat or serum did not produce wheal in either hypohidrotic or anhidrotic area. Histologically, a periglandular lymphocytic infiltrate was observed around eccrine glands in the anhidrotic but not hypohidrotic area of all patients (Figure 1d). There was no occlusion of sweat ducts. By immunohistochemistry, the infiltrating lymphocytes consisted of a mixture of $CD4^+$ and $CD8^+$ T cells (CD4/CD8 ratio, 1.21; Figure 1e).

Skin sections were immunohistochemically stained with anti-cholinergic receptor muscarin 3 (CHRM3) antibody (H-210, 1:50; Santa Cruz Biotechnology), which is the most important CHR for sweating (Schiavone and Brambilla, 1991). Eccrine epithelial cells of a normal subject expressed CHRM3 (Figure 2a, left) as well as the epidermis and hair follicle cells (Kurzen *et al.*, 2004). Although the cells in the hypohidrotic area bore CHRM3 at lower but moderate levels (Figure 2a, middle), no staining was seen in the anhidrotic areas (Figure 2a, right). Digitalized specimens were exported to JPG files by NDP view software (Hamamatsu Photonics, Hamamatsu, Japan), and three different areas of the cytoplasm of eccrine epithelial cells were expressed as "red density" (RD) (Hino *et al.*, 2010). CHRM3 expression was significantly lower in the anhidrotic than hypohidrotic areas (Figure 2b). However, specificity is the major issue in this immunohistochemical study. Therefore, real-time PCR was performed. Total RNA from serial sections was extracted in cases 1, 2, and 4 and reverse transcribed into complementary DNA using the Qiagen RNeasy FFPE Kit (Qiagen, Hilden, Germany) and first-strand cDNA synthesis kit RT-PCR (Roche Diagnostics, Indianapolis, IN). The expression levels of *CHRM3* and control *GAPDH* (*glyceraldehyde-3-phosphate dehydrogenase*) were examined using ×20 Assays-on-Demand Gene Expression Assay Mix (Hs00265216_s1 and Hs00266705_g1, respectively; Applied Biosystems, Foster City, CA). We performed PCR using RNAs without reverse transcriptase step for each sample. As represented in Figure 2d, we did not amplify the *CHRM3* gene from any RNA without reverse transcriptase (lane 1), but reverse transcriptase step yielded PCR products at an expected size 72 bp (lane 2), revealing that positive *CHRM3* PCR results of real-time PCR were not derived from contaminated genomic DNA. The levels of *CHRM3* expression were higher in the hypohidrotic than anhidrotic areas (Figure 2e).

As mast cells produce histamine in response to acetylcholine (Fantozzi

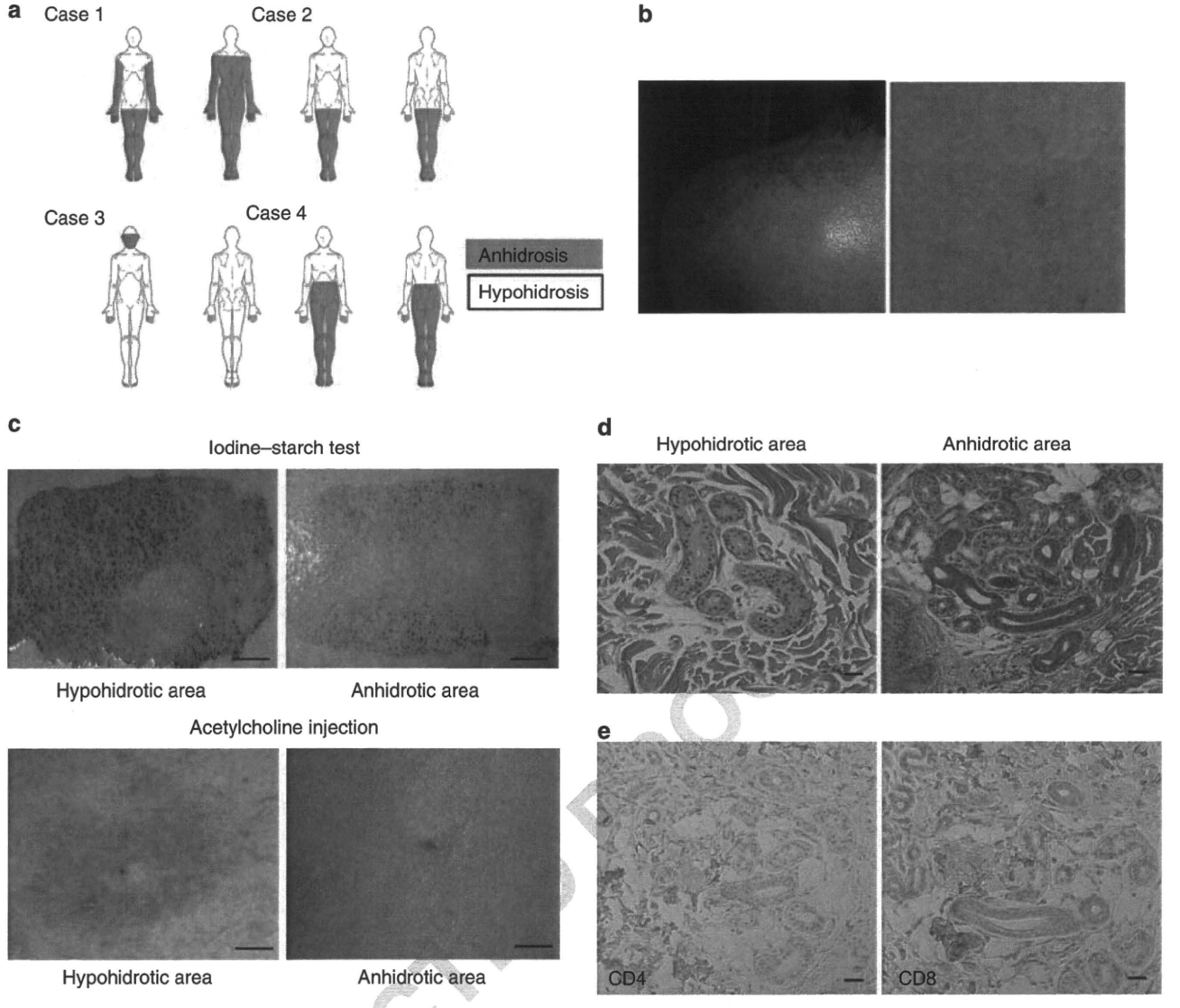

Figure 1. Clinical and histological studies. (**a**) Anhidrotic and hypohidrotic areas in each case. (**b**) Left: Iodine–starch test in case 1. Whereas the applied iodine–starch was discolored by sweat on the left shoulder (hypohidrotic area), such a black color change was not seen on the back, indicating the complete absence of sweating (anhidrotic area). Right: Exercise challenge induced wheals that coincided with sweat orifice on the hypohidrotic area. (**c**) Acethylcholine injection test in the anhidrotic and hypohidrotic areas as represented by case 1. After determination of the anhidrotic and hypohidrotic areas by exercise challenge and iodine–starch application (upper panel), acetylcholine was injected at both sites. Wheal occurred at the hypohidrotic but not anhidrotic area (lower panel). Bar = 1 cm. (**d**) Histological microphotographs of anhidrotic and hypohidrotic areas in case 1. Biopsy specimens were taken from the anhidrotic and hypohidrotic areas (hematoxyline and eosin, original magnification × 100). Note that lymphocytes infiltrate around the sweat glands in the anhidrotic but not hypohidrotic area. Bar = 30 μm. (**e**) Immunophenotype of infiltrating lymphocytes. The infiltrating lymphocytes were immunohistochemically stained for CD4 (left) and CD8 (right). Bar = 30 μm.

et al., 1978; Blandina *et al.*, 1980), we investigated CHR expression in mast cells just in vicinity of eccrine glands. Serial sections were alternatively stained with toluidine blue and with anti-CHRM3 antibody. Mast cells were identified by positive toluidine blue staining (Figure 2c, upper panel), and CHRM3 expression by mast cells was examined in the antibody-stained adjacent sections (Figure 2c, lower panel). In a normal control, mast cells expressed CHRM3 at high levels. Mast cells in conjunction with the secretory portion expressed CHRM3 in the hypohidrotic but not anhidrotic areas. There was no significant difference in the number of mast cells between the anhidrotic and hypohidrotic areas.

Our study revealed that the skin of patients with CUAH is divided into the wheal-non-occuring anhidrotic and wheal-occuring hypohidrotic areas. Even in the hypohidrotic areas, the intradermal injection of autologous sweat did not yield wheal, suggesting the absence of sweat allergy (Tsuchiya *et al.*, 2004). We found the lack of CHRM3 expression in the anhidrotic skin, which may lead to the lack of sensitivity to acetylcholine. Mast cells are responsible for wheal formation and present just in the vicinity of eccrine glands. Neither eccrine gland cells nor mast cells expressed CHRM3 in the anhidrotic area, and it is thus reasonable

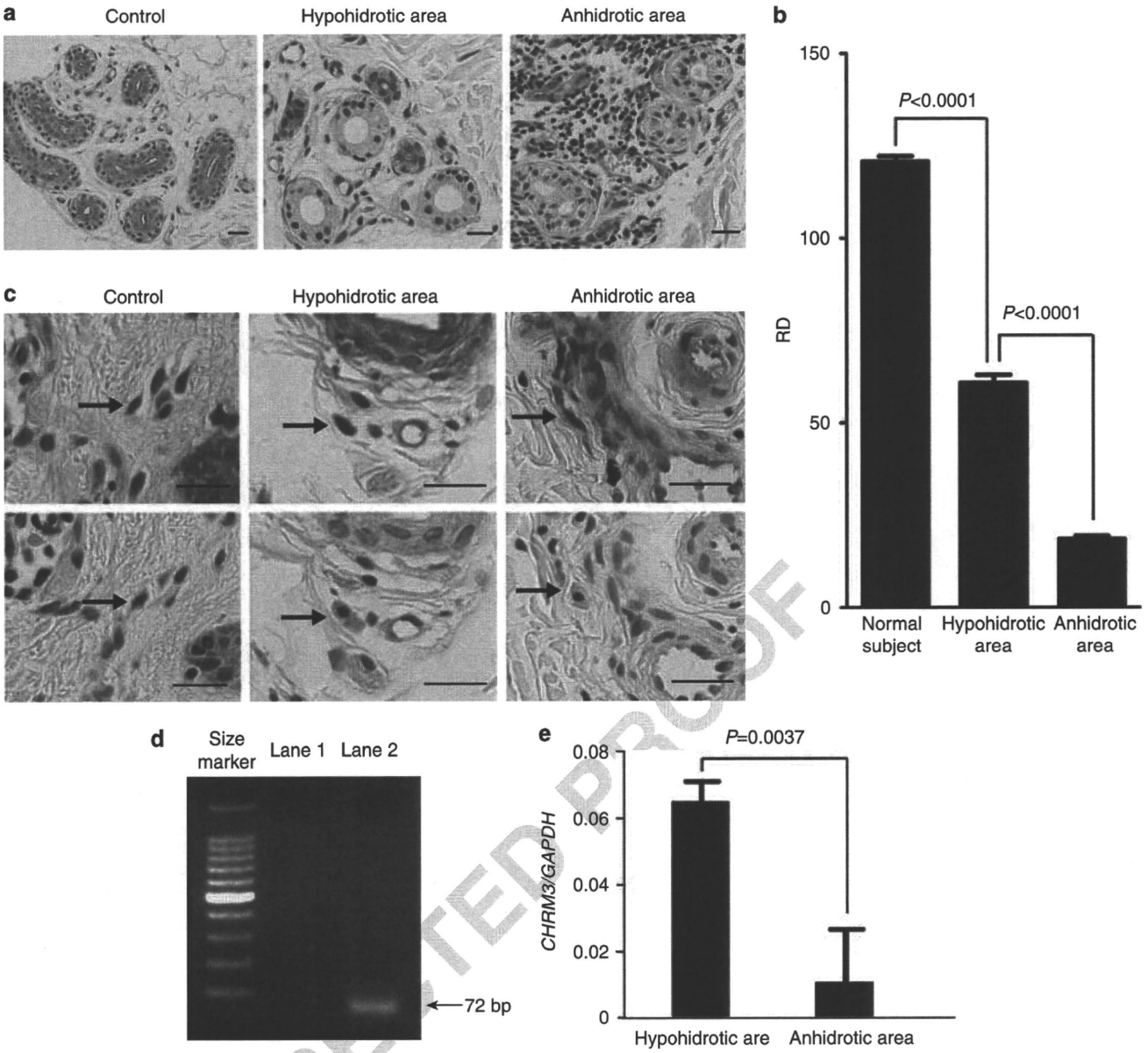

Figure 2. Expression of anti-cholinergic receptor muscarin 3 (CHRM3) in eccrine gland epithelial cells and mast cells. (**a**) CHRM3 expression in eccrine gland epithelial cells. Sections from normal subject's skin (left), and the hypohidrotic skin (middle) and anhidrotic skin (right) of case 1 were immunohistochemically stained with anti-CHRM3 antibody. Bar = 30 μm. (**b**) Staining intensity of CHRM3 expressed as "red density" (RD) in the anhidrotic and hypohidrotic areas of the four cases and in the skin of a normal subject. Three areas of eccrine epithelial cells at the anhidrotic and hypohidrotic areas in each case were subjected to RD analysis, and the mean RD intensity in each case was obtained. Then, the mean ± SD of the four cases was calculated. (**c**) CHRM3 expression in mast cells. Skin sections of a normal subject (control), the hypohidrotic and anhidrotic skin of the patients were stained with toluidine blue (upper panel) or immunohistochemically with CHRM3 (lower panel). Serial sections of each specimen were alternatively stained for CHRM3 and toluidine blue. Mast cells were identified by toluidine blue (arrows). The corresponding sections for toluidine blue and CHRM3 are adjacent. Bar = 30 μm. (**d**) mRNA expression for CHRM3. The end products of real-time PCR using RNA without reverse transcriptase reaction (lane 1) and complementary DNA (cDNA) (lane 2) from hypohidrotic skin of case 1 were electrophoresed in 1.8% agarose gel along with 100 bp DNA ladder (Takara, Kyoto, Japan). *CHRM3* gene products were recognized at an expected size, 72 bp, only in lane 2. (**e**) The expression levels of *CHRM3* and control *GAPDH* (*glyceraldehyde-3-phosphate dehydrogenase*) in the hypohidrotic and anhidrotic areas by real-time PCR analysis. Total RNA from serial sections was extracted in cases 1, 2, and 4 and reverse transcribed into cDNA and first-strand cDNA synthesis kit RT-PCR.

that sweating and wheal formation were absent in this area. CHR mediates wheal development (Tong *et al.*, 1997), and acetylcholine can induce degranulation of mast cells (Fantozzi *et al.*, 1978; Blandina *et al.*, 1980). In the hypohidrotic area, we are tempting to speculate that acetylcholine released from nerves upon exercise cannot be completely trapped by CHR of eccrine glands and overflows to the adjacent mast cells. In this scenario, mast cells may be capable of producing histamine and resultant wheal in response to acetylcholine because of the expression of some degree of CHRM3.

CONFLICT OF INTEREST

The authors state no conflict of interest.

Yu Sawada[1], Motonobu Nakamura[1], Toshinori Bito[1], Shoko Fukamachi[1], Rieko Kabashima[1], Kazunari Sugita[1], Ryosuke Hino[1] and Yoshiki Tokura[1]

[1]Department of Dermatology, University of Occupational and Environmental Health, Kitakyushu, Japan
E-mail: tokura@med.uoeh-u.ac.jp

REFERENCES

Adachi J, Aoki T, Yamatodani A (1994) Demonstration of sweat allergy in cholinergic urticaria. *J Dermatol Sci* 7:142–9

Blandina P, Fantozzi R, Mannaioni PF *et al.* (1980) Characteristics of histamine release evoked by acetylcholine in isolated rat mast cells. *J Physiol* 301:281–93

Fantozzi R, Masini E, Blandina P *et al.* (1978) Release of histamine from rat mast cells by acetylcholine. *Nature* 273:473–4

Fukunaga A, Bito T, Tsuru K *et al.* (2005) Responsiveness to autologous sweat and serum in cholinergic urticaria classifies its clinical subtypes. *J Allergy Clin Immunol* 116:397–402

Hino R, Kabashima K, Kato Y *et al.* (2010) Tumor cell expression of programmed cell death 1 ligand 1 is a prognostic factor for malignant melanoma. *Cancer* 116:1757–66

Itakura E, Urabe K, Yasumoto S *et al.* (2000) Cholinergic urticaria associated with acquired generalized hypohidrosis: report of a case and review of the literature. *Br J Dermatol* 143:1064–6

Kay DM, Maibach HI (1969) Pruritis and acquired anhidrosis; two unusual cases. *Arch Dermatol* 100:291–3

Kobayashi H, Aiba S, Yamagishi T *et al.* (2002) Cholinergic urticaria, a new pathogenic concept: hypohidrosis due to interference with the delivery of sweat to the skin. *Dermatology* 204:173–8

Schiavone A, Brambilla A (1991) Muscarinic M3 receptors mediate secretion from sweat glands in the rat. *Pharmacol Res* 23:233–9

Tong LJ, Balakrishnan G, Kochan JP *et al.* (1997) Assessment of autoimmunity in patients with chronic urticaria. *J Allergy Clin Immunol* 99:461–5

Tsuchiya T, Aoyama K, Hasegawa M *et al.* (2004) Cholinergic urticaria associated with hypohidrosis improved after admission. *Jpn J Clin Dermatol* 58:129–31

Yoshida M, Mizutani K, Watanabe D *et al.* (2009) Cholinergic urticaria associated with Idiopathic generalized anhidrosis. *Practical Dermatol* 31:41–4

DOI:10.1111/j.1600-0625.2010.01084.x
www.blackwellpublishing.com/EXD

Original Article

Ultraviolet light induces Stat3 activation in human keratinocytes and fibroblasts through reactive oxygen species and DNA damage

Toshinori Bito[1,2], Naoko Sumita[1], Taro Masaki[1], Toshiro Shirakawa[3], Masato Ueda[1], Ryutaro Yoshiki[2], Yoshiki Tokura[2] and Chikako Nishigori[1]

[1]Division of Dermatology, Department of Clinical Molecular Medicine, Kobe University Graduate School of Medicine, Kobe, Japan;
[2]Department of Dermatology, University of Occupational and Environmental Health, Kitakyushu, Japan;
[3]International Center for Medical Research and Treatment, Kobe University Graduate School of Medicine, Kobe, Japan
Correspondence: Dr Toshinori Bito, Department of Dermatology, University of Occupational and Environmental Health, 1-1 Iseigaoka, Yahatanishi-ku, Kitakyushu, 807-8555, Japan, Tel.: 81 93 691 7445, Fax: 81 93 691 0907, e-mail: bito@med.kobe-u.ac.jp

Accepted for publication 27 January 2010

Abstract: Stat3 is activated by the outer stressors, such as ultraviolet (UV) exposure. In this study, we investigated the Stat3 response to UV irradiation in human epidermal keratinocytes and dermal fibroblasts. Results indicated that UVB and UVC differentially activate Stat3 in these cells. The UV-induced Stat3 activation was mediated by both reactive oxygen species (ROS) and DNA damage, and the dominancy of ROS and DNA damage to activate Stat3 depended on the wavelength of UV. By using fibroblasts from a patient with xeroderma pigmentosum A (XP-A) and those transfected with human *XPA* gene, we found that UVB activates Stat3 *via* both ROS and DNA damage, while UVC does so mainly *via* DNA damage. The present data suggest that Stat3 activation in UV-exposed human skin is one of the initial events where DNA damage and ROS are involved.

Key words: DNA – reactive oxygen species – skin – Stat3 – UV

Please cite this paper as: Ultraviolet light induces Stat3 activation in human keratinocytes and fibroblasts through reactive oxygen species and DNA damage. Experimental Dermatology 2010; **19**: 654–660.

Introduction

In aged individuals, accumulative exposure to ultraviolet (UV) light from the sun, particularly its UVB component (290–320 nm), to the skin is a major cause for the development of skin cancers. Photoageing is caused by cumulative sun exposure in addition to chronologic ageing. To avoid photoageing including skin cancer development, the molecular mechanisms underlying UV-induced skin damage need to be elucidated. Fisher et al. have revealed that the UV irradiation activates signalling pathways such as ERK 1/2 which upregulates expression and functional activation of a nuclear transcription factor, AP-1, resulting in diverse response including photoageing (1). UV also activates NF-κB that stimulates the transcription of proinflammatory cytokine genes, which reversely acts through their surface receptors to further stimulate AP-1 and NF-κB, thereby amplifying the UV response (1). Thus, UV is suggested to be an important cue to evoke a series of biological responses *in vivo*.

Abbreviations: STAT, signal transducer and activator of transcription; UV, ultraviolet; XP, xeroderma pigmentosum.

On the other hand, a recent study has reported that UVB activates another transcription factor, signal transducer and activator of transcription 3 (Stat3) in the skin of hairless mouse (2). Stat3 has been expected as a target for the management of skin cancer. Signal transducers and activators of transcription (STATs) are activated in response to a variety of cytokines and growth factors. The STAT family has seven known members in mammals, Stat1, Stat2, Stat3, Stat4, Stat5a, Stat5b and Stat6. Among the STATs, Stat3 has been implicated to have a potential to prevent apoptotic signalling in cells (3). Sano et al. have reported that Stat3 activation rescues the UVB-induced apoptosis of keratinocytes in hairless mouse (4). As the previous studies revealed the constitutive activation of Stat3 in various human cancers (5–7), Stat3 is recognized as an oncogene (8). These various observations have led to the current concept that Stat3 plays a more important role than does AP-1 or NF-κB for photocarcinogenesis. However, the roles of Stat3 in the human skin and relating disorders remain unclear. Previously, we have reported that the inhibition of Stat3 activity is not sufficient to induce apoptosis, although Stat3 activation is required for cell proliferation and tumorigenesis for cutaneous squamous cell

carcinoma (9). Accumulated evidence supports that Stat3 activation prevents the cell death from various damage including UV. Human cells are protected from a variety of external stressor by activating Stat3, resulting in enhancement of survival. Nevertheless, excess activation of Stat3 may also yield unexpected outcomes such as cancer.

In this study, we investigated the initial signalling pathway following UV irradiation in human epidermal keratinocytes and dermal fibroblasts, focusing on Stat3. To further address the mechanism underlying the UVB-induced Stat3 activation, human fibroblasts from a patient with xeroderma pigmentosum A (XP-A) having repair deficiency in UV-induced DNA damage were also subjected. Results indicate that Stat3 is activated by UVB in human keratinocytes and fibroblasts in a different manner.

Materials and methods

Cells, cell culture and treatment

Primary normal human epidermal keratinocytes (HEK) and normal fibroblasts were purchased from KURABO (Osaka, Japan). HEK were grown in keratinocyte serum–free medium supplemented with human keratinocyte growth supplement and penicillin, streptomycin and amphotericin B (PSA) solution (Gibco, Grand Island, NY, USA). Primary human fibroblasts were obtained from a patient with XP-A, after obtaining a written informed consent, and was designated XP1MG (10). They were grown in Dulbecco's modified Eagle's minimum essential medium (Invitrogen Co., Carlsbad, CA, USA) supplemented with 15% foetal bovine serum (HyClone, Logan, UT, USA) and maintained in a humidified air containing 5% CO_2 at 37°C. The regular medium for the both cells was replaced with the medium without growth supplement, PSA or serum 24 h before UV irradiation. Buthionine sulfoximine (BSO) and (±) α-lipoic acid (LA) were purchased from Sigma Chemicals Co. (St Louis, MO, USA). BSO was freshly dissolved in DMSO at 100 mM. LA was prepared in distilled water at 50 mM, and adjusted with 1 M NaOH to pH8.0. HEK were pretreated with 100 μM of BSO or 500 μM of LA for 24 h before UV exposure. After nine of 10-ml medium was removed, cells were irradiated with UV and replaced with the medium containing LA immediately after the exposure. UV-absorbance of LA of our working condition was recorded from 260 to 390 nm using a Beckman DU-70 spectrophotometer.

UV irradiation

FL20SE fluorescent lumps (Toshiba Electric Co., Tokyo, Japan) were used as a source of UVB. These lamps emit mainly wavelengths between 280 and 360 nm, peaking at 311 nm. Flux intensity was measured with an UVR-305/365D UV radiometer (Tokyo Optical Co Ltd, Tokyo, Japan). Germicidal lamps predominantly emitting 254 nm (GL10; Toshiba Electric Co.) were used as a source of UVC. Fluence rates were measured by the UV radiometers, UV-254 (Topcon; Tokyo Kogaku Kikai KK, Tokyo, Japan).

Electrophoretic mobility shift assay

Nuclear extracts from the cells were prepared following the method described by Corsini et al. (11), with slight modifications. Electrophoretic mobility shift assay (EMSA) was performed essentially as described earlier (12). Binding reaction mixtures (20 μl) containing 5 μg nuclear extract protein, 2 μg poly (dI-dC) (Amersham Pharmacia Biotech, Piscataway, NJ, USA), ^{32}P-labelled probe (Stat3), 50 mM NaCl, 2 mM $MgCl_2$, 0.2 mM Na_2EDTA, 1 mM DTT, 10% (v/v) glycerol and 4 mM Tris–HCl (pH 7.9) were incubated for 30 min at room temperature. Proteins were separated by electrophoresis in native 6% polyacrylamide gels using a Tris-borate-EDTA running buffer (12.5 mM Tris-borate containing 0.25 mM Na_2EDTA, pH 8.0), followed by autoradiography. The Stat3 probe (Santa Cruz Biotechnology, Santa Cruz, CA, USA) was labelled with [γ-^{32}P] dATP (Du Pont NEN, Boston, MA, USA) using T4 polynucleotide kinase (Boehringer MannheimRoche, Mannheim, Germany).

Immunoblot analysis

Cells were washed with ice-cold D-PBS containing 200 μM sodium orthovanadate (Na_3VO_4), frozen immediately in liquid nitrogen, and then lysed in lysis buffer (25 mM Tris–HCl, pH 7.6, 200 mM boric acid, 150 mM NaCl, 50 mM NaF, 5 mM Na_2EDTA, 1% Triton X-100, 10 mM sodium pyrophosphate, 2 mM EGTA, 20 mM p-nitrophenyl phosphate, 1% BSA, 20 μM Na_3VO_4 and 2 mM DTT) containing protease inhibitors (2 μg/ml each of aprotinin, leupeptin, pepstain, antipain and 100 μg/ml PMSF). The lysates were centrifuged at 10 000 × *g* at 4°C for 15 min, and the resulting supernatants were subjected to immunoblot analysis. Protein concentrations in the supernatants were quantitated by the Coomassie® plus protein assay reagent (Bio-Rad). Samples (20 μg protein each) for immunoblotting were separated on 8% polyacrylamide gels for Stat3 by SDS–polyacrylamide gel electrophoresis and were blotted onto Hybond-ECL nitrocellulose membranes (Amersham Pharmacia Biotech). The membranes were blocked with 5% skim milk in Tris-buffered saline for 2 h at room temperature and were then probed with primary polyclonal antibodies to phospho-Stat3 (p-Tyr705 or p-Ser727) antibody (Cell Signalling Technology, Beverly, MA, USA) overnight at 4°C, and then incubated with corresponding horseradish peroxidase-conjugated secondary antibodies at room temperature for 1 h. Bound antibody was detected with Immunostar Reagents (Wako, Osaka, Japan). The membranes were exposed to Hyperfilm (Amersham Pharmacia Biotech). After the film exposure, the

membranes were washed four times for 5 min each in PBS-Tween 20, and were then incubated for 30 min at 50°C in stripping buffer (62.5 mM Tris–HCl pH 6.8, 2% SDS and 100 mM 2-mercaptoethanol). The membranes were blocked with 5% skim milk again, and then reprobed with an antibody to total Stat3 protein (Cell Signalling Technology), or reblotted with human actin (Santa Cruz Biotechnology) as a loading control overnight at 4°C, and then incubated with corresponding horseradish peroxidase-conjugated secondary antibodies. Quantification of protein expression was performed using NIH image analysis software (version 1.62f) (Bethesda, MD, USA).

Immunofluorescence

Human epidermal keratinocytes were plated on Lab-Tek® chamber slides (Nalge Nunc International, Naperville, IL, USA). Two-day-cultured cells were left untreated or treated with LA for 24 h and exposed to UVB. After UV exposure, the cells were incubated for 15 min and fixed with 3% formaldehyde in PBS for 15 min at room temperature followed by permeabilization with ice-cold methanol for 10 min. The slides were rinsed in PBS and incubated for 18 h at 4°C with phospho-Stat3 (p-Tyr705 or p-Ser727) antibody (Cell Signalling Technology) diluted in 0.3% Triton X-100 in PBS following blocking in 5% normal rabbit serum for 60 min. After incubation, the slides were washed three times in PBS and incubated with fluorochrome-conjugated secondary anti-rabbit antibody for 1 h. Following two washes in PBS, the slides were mounted with Prolong® Gold Antifade Reagent (Invitrogen Co.). Fluorescence was examined by a laser scanning confocal imaging microscope and processed with LSM Image Browser (Carl Zeiss, Tokyo, Japan).

Electroporation

Plasmids containing human *XPA* gene, pcHA-*XPA*, constructed from pcDNA3 inserting *XPA* cDNA and Influenza haemaggultinin gene (HA) as a tag (kindly provided by Dr Kiyoji Tanaka), was transfected into XP1MG by an electroporation method (350 kV, 1.5 ms) using the ECM 830 electroporation system (BTX, San Diego, CA, USA). XPA protein and HA after electroporation were detected by Western blotting using monoclonal antibody against human XPA and HA. XP1MG cells transfected with pcHA-*XPA* were harvested and inoculated into 6-well cell culture plates at the density of 2×10^5 cells/well for 12 h, and then exposed to UVC. The cell lysates were utilized for immunoblotting.

Statistical analyses

Data are expressed as means ± standard deviations. Statistical analyses were performed using Prism 5 software (GraphPad Software, San Diego, CA, USA). Unpaired experimental groups were compared with the Student's *t*-test. $P < 0.05$ was considered significant.

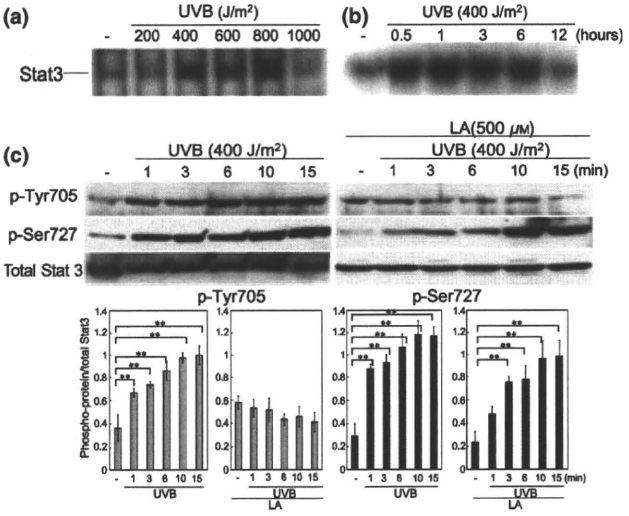

Figure 1. UVB-induced DNA binding activity and phosphorylation of Stat3 in human epidermal keratinocytes (HEK). Nuclear extracts from the cells under the regular condition were analysed using EMSA with a ^{32}P-labelled DNA probe to detect DNA binding activity of Stat3. (a) HEK were collected 30 min after UVB irradiation, and nuclear extracts were subjected to EMSA. (b) A kinetics analysis was performed after 400 J/m^2 of UVB irradiation. Data are a representative of three independent experiments. (c) HEK were exposed to 400 J/m^2 of UVB without or with 500 μM of LA pretreatment for 24 h and collected at the indicated time points. The cell lysates (20 μg) were immunoblotted with each of the anti-p-Stat3 (p-Tyr705) antibody, or p-Stat3 (p-Ser727) antibody and reprobed with an anti-Stat3 (total) antibody as a loading control. Data are a representative of three independent experiments. The bar graphs are expressed as the relative ratio of phospho-Stat3 protein expression to total Stat3 protein expression by densitometry using NIH image analysis software. Data are mean ± SD of three independent experiments. $^{**}P < 0.01$ are statistically significant when compared with the non-treated control.

Results

UVB-induced Stat3 activation in HEK

Stat3 DNA binding activity was examined following single UVB exposure in HEK. HEK were exposed to UVB and collected 30 min later. Nuclear extracts from the cells were analysed by EMSA. Stat3 was activated in a dose-dependent manner from 400 to 800 J/m^2 of UVB irradiation (Fig. 1a). A kinetics analysis was performed following 400 J/m^2 of UVB irradiation. Stat3 was activated 30 min after UVB irradiation, and its activation continued for 6 h and returned to the baseline 12 h after UVB exposure (Fig. 1b).

UVB upregulated Stat3 phosphorylation at both Tyr705 and Ser727 and antioxidants suppressed UVB-induced Stat3 activation markedly at Tyr705 and partially at Ser727

Stat3 activation requires the phosphorylation at both tyrosine 705 (Tyr705) and serine 727 (Ser727) in stimulation with cytokines or growth factors. Therefore, we investigated

the phosphorylation of Tyr705 and Ser727 of Stat3 in UVB-exposed HEK by immunoblot analysis. HEK were irradiated with 400 J/m^2 of UVB and harvested at 1, 3, 6, 10 and 15 min after UVB irradiation. The cell lysates (20 μg) were immunoblotted with an anti-p-Stat3 (p-Tyr705), or p-Stat3 (p-Ser727) antibody and reprobed with an anti-Stat3 (total) antibody as a loading control. Both p-Tyr705 and p-Ser727 protein levels were upregulated at 1 min after UVB irradiation, and that upregulation continued at least for 15 min (Fig. 1c, left panel).

UVB is well known to generate reactive oxygen species (ROS), whereas UVC generates little amount of ROS (13). The cellular level of glutathione (GSH), which carries scavenge system for ROS in cells, can be elevated by lipoic acid (LA), a precursor of GSH. To verify the influence of ROS, HEK were pretreated with antioxidants, LA (500 μM) for 24 h and exposed to UVB under the same condition as was performed without LA. LA treatment suppressed the UVB-induced upregulation of p-Tyr705 at all the time points examined, but LA treatment suppressed the UVB-induced p-Ser727 only slightly (Fig. 1c, right panel). The absorbance of LA at this range was almost negligible at our experimental condition. In addition, flux intensity was measured using UV radiometer through the medium with or without LA at the concentration. Each medium showed the same intensity as 0.98 mW/cm^2. An immunofluorescence analysis further supported the differential phosphorylation of Tyr705 and Ser727 in keratinocytes (Fig. 2). The protein expression of p-Tyr705 was seen both in the nuclei and in the cytoplasm 15 min after 400 J/m^2 of UVB, and again the protein

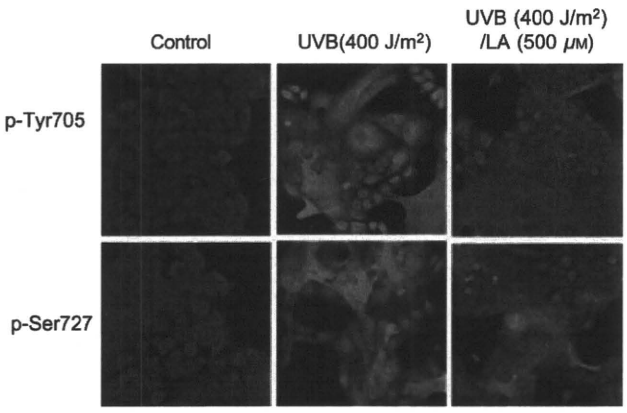

Figure 2. Localization of phosphorylated forms of Tyr705 and Ser727 following UVB irradiation. human epidermal keratinocytes were plated on the chamber slides. The cells after 2 days of culture were left untreated or treated with LA for 24 h and then exposed to 400 J/m^2 of UVB. The protein expression of p-Tyr705 or p-Ser727 was examined using a laser scanning confocal imaging microscope in fluorescence 15 min after UVB irradiation. The protein expression of p-Tyr705 was seen in both the nuclei and the cytoplasm, and the protein expression was suppressed with 500 μM of LA pretreatment. The protein expression of p-Ser727 was seen predominantly in the nulcei, and LA pretreatment exerted a weak suppression.

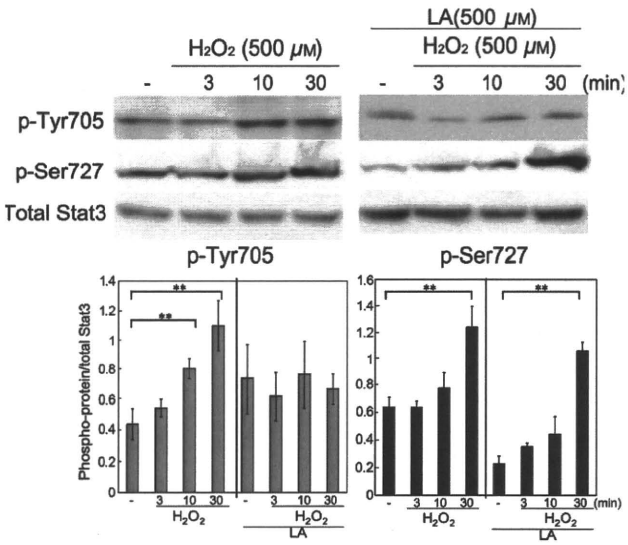

Figure 3. Hydrogen peroxide-induced Stat3 phosphorylation at both Tyr705 and Ser727 sites. human epidermal keratinocytes were incubated with 500 μM hydrogen peroxide (H_2O_2) without or with LA pretreatment for the indicated time. Data are a representative of three independent experiments. The bar graphs are expressed as the relative ratio of phospho-Stat3 protein expression to total Stat3 protein expression by densitometry using NIH image analysis software. Data are mean ± SD of three independent experiments. $^{**}P < 0.01$ are statistically significant when compared with the non-treated control.

expression was suppressed by LA treatment. On the other hand, the expression of p-Ser727 was seen dominantly in the nulcei at the same time points after 400 J/m^2 of UVB, and LA treatment had little effect on the expression. Virtually no phospho-Stat3 protein was detected in HEK without stimuli. Next, to examine whether ROS activate Stat3 in HEK, HEK were incubated with hydrogen peroxide (H_2O_2) for the indicated period. Treatment with 500 μM of H_2O_2 for 10 and 30 min activated Stat3 on Tyr705, whereas Ser727 activation was observed only after 30 min treatment (Fig. 3). Pretreatment with LA abrogated the H_2O_2-induced upregulation of p-Tyr705 throughout the time course, but failed to abrogate the Ser727 phosphorylation (Fig. 3).

Phosphorylation of Stat3 by UVC at Ser727

UVB irradiation produces both DNA damage and membrane damage. To elucidate the mechanism of UVB-induced Stat3 activation, we employed UVC irradiation because UVC is known to preferentially cause DNA damage such as pyrimidine dimer and (6-4) CT photoproduct (13). Although our skin is not exposed to UVC irradiation, we used UVC as a procedure for DNA damage, while H_2O_2 served as a tool for membrane damage. HEK were irradiated with single exposure of UVC and were collected at 1, 3, 6, 10 and 15 min after UVC irradiation. P-Tyr705 was slightly upregulated at 6 and 10 min after UVC irradiation, but UVC totally caused little affect on p-Tyr705 protein (Fig. 4). On the other hand,

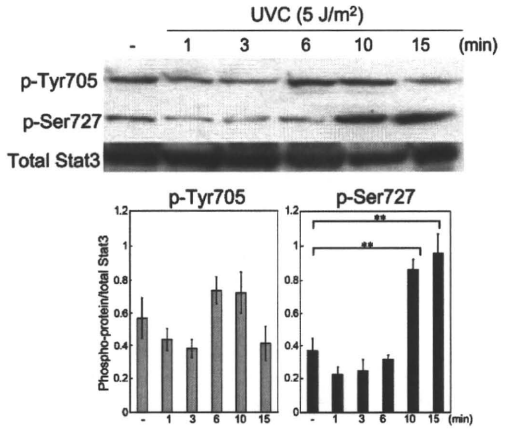

Figure 4. UVC-induced Stat3 phosphorylation at Ser727 site. human epidermal keratinocytes were irradiated with 5 J/m^2 of UVC and collected at the indicated time points. The cell lysates (20 μg) were immunoblotted with each of the anti-p-Stat3 (p-Tyr705) antibody, or p-Stat3 (p-Ser727) antibody and reprobed with an anti-Stat3 (total) antibody as a loading control. Data are a representative of three independent experiments. The bar graphs are expressed as the relative ratio of phospho-Stat3 protein expression to total Stat3 protein expression by densitometry using NIH image analysis software. Data are mean ± SD of three independent experiments. $^{**}P < 0.01$ are statistically significant when compared with the non-treated control.

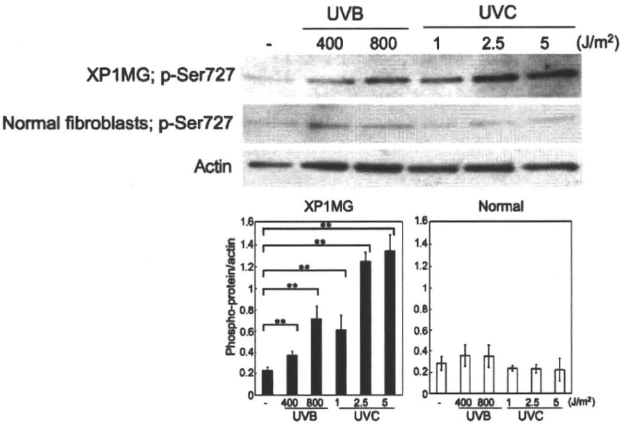

Figure 5. Phosphorylation of Stat3 by UVB or UVC irradiation in XP-A fibroblasts but not in normal fibroblasts. XP1MG fibroblasts or normal fibroblasts were irradiated by UVB (400 or 800 J/m^2) or UVC (1, 2.5 or 5 J/m^2) and collected 10 min after irradiation. The cell lysates (20 μg) were immunoblotted with anti-p-Stat3 (p-Ser727) antibody and reblotted with human actin as a loading control. Data are a representative of three independent experiments. The bar graphs are expressed as the relative ratio of phospho-Stat3 protein expression to actin protein expression by densitometry using NIH image analysis software. Data are mean ± SD of three independent experiments. $^{**}P < 0.01$ are statistically significant when compared with the non-treated control.

p-Ser727 was clearly elevated at 10 and 15 min. As UVB up-regulated p-Ser727 protein earlier than UVC, each wavelength might exert phosphorylation in different mechanisms. BSO depletes cellular GSH and renders cells sensitive to ROS (14). The balance between the production rate of ROS and the function of GSH affects the intracellular reduction–oxidation status, which is crucial for the regulation of several cellular physiological functions. To assess the role of ROS in the UVC-induced Stat3 activation, the effect of LA and sub-lethal concentrations of BSO was examined. HEK were pre-treated with LA (500 μM) or 100 μM of BSO and exposed to 5 J/m^2 of UVC. Phosphorylation levels neither at Tyr705 nor at Ser727 was affected by LA or BSO pretreatment (data not shown).

Upregulation of phospho-Stat3 at Ser727 by UVB and UVC in XP1MG fibroblasts

XP-A is an inheritated photosensitive disorder caused by repair deficiency in UV-induced DNA damage, and the responsible gene for XP-A is involved in DNA damage recognition in nucleotide excision repair (15). To ask whether pyrimidine dimer, major UV-induced DNA damage can be a trigger for Stat3 activation, Stat3 activity was examined using cells from a XP-A patient. Because keratinocytes from XP patients are neither commercially available nor available from the patient. We used the fibroblasts from the XP-A patient. Stat3 activation was compared between XP1MG, a fibroblast from a XP-A patient, and normal fibroblasts after UVB or UVC irradiation. No significant increase in Stat3 protein was observed in normal fibroblasts by 800 J/m^2 of UVB or 5 J/m^2 of UVC, whereas normal keratinocytes showed phosphorylation at Ser727 by the same doses of UVB and UVC (as shown in Figs 1c and 4). Fibroblasts look less responsive to UV damage in comparison with keratinocytes. However, single UVB or UVC irradiation dose-dependently induced Stat3 phosphorylation at Ser727 in XP1MG (Fig. 5). As for phosphorylation of Tyr705, no activation could be observed in XP1MG or normal fibroblasts by the same dose of UV, indicating that Ser727 was more sensitive to UV irradiation than Tyr705 in the fibroblasts (data not shown). To verify whether UV activates Ser727 of Stat3 through the DNA damages in XP1MG, pcHA-*XPA* was transfected into XP1MG. pcDNA3 was used as a control vector. Transfection of the *XPA* gene almost completely abrogated the UVC upregulation of Stat3 phosphorylated protein on Ser727, whereas the UVB-induced Stat3 phosphorylation was partially reduced (Fig. 6).

Discussion

We found that UVB activates Stat3 in human keratinocytes and fibroblasts in a manner different from each other. The UV-induced Stat3 phosphorylation is mediated by both ROS and DNA damage produced depending on the wavelength of UV. Accordingly, Grether-Beck et al. have shown that both UVA and UVB activate transcription factors such as AP1, AP2 or NF-κB in different manners (16).

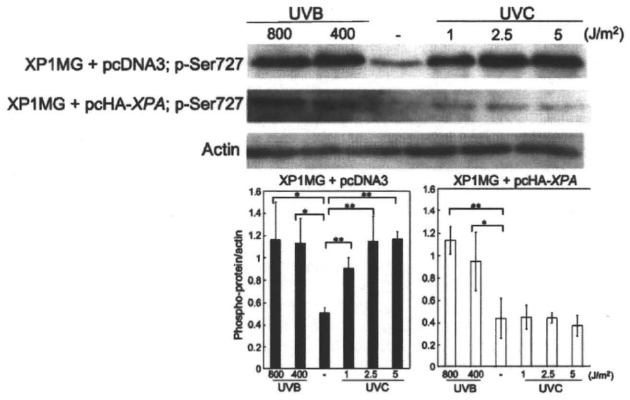

Figure 6. Transfection with *XPA* gene abrogated the UV-induced phosphorylation of Stat3 in XP1MG. XP1MG transfected with pcHA-*XPA* or control vector (pcDNA3) were irradiated with UVB (400 or 800 J/m^2) or UVC (1, 2.5 or 5 J/m^2) and were collected 10 min after irradiation. The cell lysates (20 μg) were immunoblotted with anti-p-Stat3 (p-Ser727) antibody and reblotted with human actin as a loading control. Data are a representative of three independent experiments. The bar graphs are expressed as the relative ratio of phospho-Stat3 protein expression to actin protein expression by densitometry using NIH image analysis software. Data are mean ± SD of three independent experiments. $*P < 0.05$ and $**P < 0.01$ are statistically significant when compared with the non-treated control.

Fisher et al. demonstrated that the activation of AP-1 and NF-κB mediates signalling pathways starting within 1 h after UV irradiation and reaches to the maximal within 4 h in human skin *in vivo* (1,17). On the other hand, Grether-Beck et al. have shown that both UVA and UVB induce an early activation observed immediately 30 min after UV treatment (16). The upregulation of Stat3 DNA binding activity was observed within 30 min after UVB irradiation in this study. In a specified condition, Simon et al. have shown that UVB is able to activate NF-κB in cytosolic extracts 20 min after treatment (18). Stat3 activation might precede AP-1 and NF-kB activation according to the situation, although it was difficult to compare it under the same condition. Our immunoblot analysis supported this notion, because Stat3 phosphorylation started within 1 min after UVB irradiation. Several previous reports using human or mouse skin *in vivo*, or *in vitro* have shown that the transcription factors are activated with UV or cytokine stimulation in a couple of hours (1,2,19,20). As far as we know, there have been no data showing such an immediate activation of transcription factors as Stat3 observed in this study. Stat3 is activated *via* the related kinases or cytokines such as epidermal growth factor receptor and IL-6 (21), and thus its activation seems to be mediated by the signalling pathways through cytokines or membrane receptors. Because of its rapid upregulation, however, UVB is suggested to activate Stat3 directly.

In this study, we found that DNA damage induces Stat3 phosphorylation. As UVC has a more potent ability to form DNA damage than UVB (22,23), we also used UVC to exclusively produce DNA damage. The similar effect of UVC to UVB on the upregulation of Stat3 protein was observed, although a slight delay of the response was seen by UVC. The pretreatment of LA diminished the UVB-induced Stat3 activation. Morphological observations by immunohistochemical method revealed that the protein expression of p-Tyr705 and p-Ser727 Stat3 was present in the cytoplasm and nuclei in the keratinocytes. The potent suppressive effect of an antioxidant, LA, on phosphorylation at Tyr 705 was clearly shown in the experiment using H_2O_2 as a stimulus, strongly suggesting the involvement of ROS in the phosphorylation at this site. The earlier phosphorylation at Ser727 was induced by UVB rather than UVC in keratinocytes, whereas the enhanced phosphorylation at Ser727 was not seen in the UVC-irradiated keratinocytes even under the ROS-sensitive condition using BSO. The timing of the UVB-induced p-Ser727 upregulation in the LA-treated cells was similar to UVC-induced Stat3 activation. Therefore, the phosphorylation at Ser727 seems to be mediated by both DNA damage and ROS. On the other hand, the phosphorylation at Tyr705 seems to be evoked mainly by ROS, which is yielded by UVB but not substantially by UVC. In this scenario, the upregulation by ROS may precede that by DNA damage on the Stat3 activation, which is consistent with our findings that Ser727 follows Tyr705 in the phosphorylation. Considering that precursors of ROS exist ubiquitously in cells, it appears that influence of ROS responded earlier than that of DNA damage in the phosphorylation. The delayed phosphorylation with H_2O_2 may be attributed to the difference between the extra- and intracellular ROS. In comparison with ROS, DNA damage induces the delayed phosphorylation presumably because of the indirect signalling pathway for the Stat3 activation.

While normal fibroblast showed little Stat3 upregulation by UVB and UVC irradiation at the same doses that HEK does, the upregulation of phospho-Stat3 protein by UV was seen in a dose-dependent manner in fibroblasts from a XP-A patient. To ask whether (i) the different responses in UV-induced Stat3 phosphorylation between normal and XP-A fibroblasts are attributed to the different abilities of DNA repair and (ii) the resultant difference in the amount of DNA damage in XP-A cells, XP-A fibroblasts were transfected with the *XPA* gene. XP1MG transfected with pcHA-*XPA* showed much lower responses to UVB and UVC in the Stat3 phosphorylation than XP1MG cells transfected with control vector, pcDNA3. The study using the transfected XP-A cells also supports the finding that Stat3 activation is induced by UVB *via* ROS and DNA damage and UVC largely *via* DNA damage. Stat3 activation operates upon cell proliferation to survive cellular damage under physiological UVB exposure, whereas deactivation of Stat3 through a rapid dephosphorylation of Tyr705 results in downregulation of anti-apoptotic molecules such as Bcl-xL

following excess UVB irradiation (9,24). Our data presented here are consistent with these findings.

Stat3 DNA binding activity is declined by 1000 J/m^2 of UVB exposure, which clinically evokes sunburn on human skin. Presumably, it is a self-defensive mechanism to eliminate the severely damaged cells by downregulating the anti-apoptotic pathway. Stat3 appears to promote cells to apoptosis in a way similar to that of tumor suppressor gene, p53 (25). Previously, we have demonstrated the downregulation of anti-apoptotic genes such as Bcl-2 or Bcl-xL by inhibition of Stat3 activation using RNA interference (9). Knezevic et al. have indicated the new UVB-induced signalling pathways to Bcl-2 of DNA photoproducts (e.g. cyclobutane pyrimidine dimer), which is an indirect and smaller component of the UV response than that of the P53-E2f1 pathway (25). Similarly, a new pathway mediated by DNA damage may play a critical role for Stat3 activation as a key regulator of UV responsiveness.

It has been shown that Stat3 activation contributes to biological activities, such as survival and maintenance of homeostasis (8). As Stat3 plays a pivotal role in cell proliferation and migration, it upregulates human telomerase reverse transcriptase (TERT) expression in both normal and tumor cells (26). An anti-ageing effect through TERT activity was observed under a cancer-resistant condition (27). Recently UV-induced skin ageing has been particularly reviewed from various viewpoints (28). Our observations in this study also suggest that Stat3 activation is one of the physiological responses to recover the photoageing in the senescence. The study of the mechanism of Stat3 activation could be helpful for a better understanding of the UV-induced skin ageing.

This study suggests that Stat3 activation in UV-exposed human skin is one of the initial events where DNA damage and ROS are involved and implies that Stat3 plays a critical role in the induction of apoptosis or senescence in response to UV. These findings regarding Stat3 may provide strategies to prevent photocarcinogenesis and photoageing.

Acknowledgements

This work was supported in part by Grants-in-Aid from the Ministry of Education, Culture, Sports, Science and Technology, Japan. We thank Mikuni Horie and Mio Hayashi for their excellent technical support.

Conflict of interest

The authors state no conflict of interest.

References

1 Fisher G J, Kang S, Varani J *et al.* Mechanisms of photoaging and chronological skin aging. Arch Dermatol 2002: **138**: 1462–1470.
2 Ahsan H, Aziz M H, Ahmad N. Ultraviolet B exposure activates Stat3 signaling via phosphorylation at tyrosine705 in skin of SKH1 hairless mouse: a target for the management of skin cancer? Biochem Biophys Res Commun 2005: **333**: 241–246.
3 Shen Y, Devgan G, Darnell J E Jr, Bromberg J F. Constitutively activated Stat3 protects fibroblasts from serum withdrawal and UV-induced apoptosis and antagonizes the proapoptotic effects of activated Stat1. Proc Natl Acad Sci U S A 2001: **98**: 1543–1548.
4 Sano S, Chan K S, Kira M *et al.* Signal transducer and activator of transcription 3 is a key regulator of keratinocyte survival and proliferation following UV irradiation. Cancer Res 2005: **65**: 5720–5729.
5 Mora L B, Buettner R, Seigne J *et al.* Constitutive activation of Stat3 in human prostate tumors and cell lines: direct inhibition of Stat3 signaling induces apoptosis of prostate cancer cells. Cancer Res 2002: **62**: 6659–6666.
6 Murakami Y, Nakano S, Niho Y, Hamasaki N, Izuhara K. Constitutive activation of Jak-2 and Tyk-2 in a v-Src-transformed human gallbladder adenocarcinoma cell line. J Cell Physiol 1998: **175**: 220–228.
7 Kube D, Holtick U, Vockerodt M *et al.* STAT3 is constitutively activated in Hodgkin cell lines. Blood 2001: **98**: 762–770.
8 Bromberg J F, Wrzeszczynska M H, Devgan G *et al.* Stat3 as an oncogene. Cell 1999: **98**: 295–303.
9 Sumita N, Bito T, Nakajima K, Nishigori C. Stat3 activation is required for cell proliferation and tumorigenesis but not for cell viability in cutaneous squamous cell carcinoma cell lines. Exp Dermatol 2006: **15**: 291–299.
10 Nishigori C, Moriwaki S, Takebe H, Tanaka T, Imamura S. Gene alterations and clinical characteristics of xeroderma pigmentosum group A patients in Japan. Arch Dermatol 1994: **130**: 191–197.
11 Corsini E, Terzoli A, Bruccoleri A, Marinovich M, Galli C L. Induction of tumor necrosis factor-alpha *in vivo* by a skin irritant, tributyltin, through activation of transcription factors: its pharmacological modulation by anti-inflammatory drugs. J Invest Dermatol 1997: **108**: 892–896.
12 Roy S, Sen C K, Kobuchi H, Packer L. Antioxidant regulation of phorbol ester-induced adhesion of human Jurkat T-cells to endothelial cells. Free Radic Biol Med 1998: **25**: 229–241.
13 Herrling T, Jung K, Fuchs J. Measurements of UV-generated free radicals/reactive oxygen species (ROS) in skin. Spectrochim Acta A Mol Biomol Spectrosc 2006: **63**: 840–845.
14 Schraufstatter I U, Hinshaw D B, Hyslop P A, Spragg R G, Cochrane C G. Glutathione cycle activity and pyridine nucleotide levels in oxidant-induced injury of cells. J Clin Invest 1985: **76**: 1131–1139.
15 Kuraoka I, Morita E H, Saijo M *et al.* Identification of a damaged-DNA binding domain of the XPA protein. Mutat Res 1996: **362**: 87–95.
16 Grether-Beck S, Olaizola-Horn S, Schmitt H *et al.* Activation of transcription factor AP-2 mediates UVA radiation- and singlet oxygen-induced expression of the human intercellular adhesion molecule 1 gene. Proc Natl Acad Sci U S A 1996: **93**: 14586–14591.
17 Fisher G J, Talwar H S, Lin J *et al.* Retinoic acid inhibits induction of c-Jun protein by ultraviolet radiation that occurs subsequent to activation of mitogen-activated protein kinase pathways in human skin *in vivo*. J Clin Invest 1998: **101**: 1432–1440.
18 Simon M M, Aragane Y, Schwarz A, Luger T A, Schwarz T. UVB light induces nuclear factor kappa B (NF kappa B) activity independently from chromosomal DNA damage in cell-free cytosolic extracts. J Invest Dermatol 1994: **102**: 422–427.
19 Huang C, Zhang D, Li J, Tong Q, Stoner G D. Differential inhibition of UV-induced activation of NF kappa B and AP-1 by extracts from black raspberries, strawberries, and blueberries. Nutr Cancer 2007: **58**: 205–212.
20 Dhanalakshmi S, Mallikarjuna G U, Singh R P, Agarwal R. Dual efficacy of silibinin in protecting or enhancing ultraviolet B radiation-caused apoptosis in HaCaT human immortalized keratinocytes. Carcinogenesis 2004: **25**: 99–106.
21 Gao S P, Mark K G, Leslie K *et al.* Mutations in the EGFR kinase domain mediate STAT3 activation via IL-6 production in human lung adenocarcinomas. J Clin Invest 2007: **117**: 3846–3856.
22 Koch-Paiz C A, Amundson S A, Bittner M L, Meltzer P S, Fornace A J Jr. Functional genomics of UV radiation responses in human cells. Mutat Res 2004: **549**: 65–78.
23 Cadet J, Sage E, Douki T. Ultraviolet radiation-mediated damage to cellular DNA. Mutat Res 2005: **571**: 3–17.
24 Sano S, Chan K S, DiGiovanni J. Impact of Stat3 activation upon skin biology: a dichotomy of its role between homeostasis and diseases. J Dermatol Sci 2008: **50**: 1–14.
25 Knezevic D, Zhang W, Rochette P J, Brash D E. Bcl-2 is the target of a UV-inducible apoptosis switch and a node for UV signaling. Proc Natl Acad Sci U S A 2007: **104**: 11286–11291.
26 Konnikova L, Simeone M C, Kruger M M, Kotecki M, Cochran B H. Signal transducer and activator of transcription 3 (STAT3) regulates human telomerase reverse transcriptase (hTERT) expression in human cancer and primary cells. Cancer Res 2005: **65**: 6516–6520.
27 Tomas-Loba A, Flores I, Fernandez-Marcos P J *et al.* Telomerase reverse transcriptase delays aging in cancer-resistant mice. Cell 2008: **135**: 609–622.
28 Berneburg M, Trelles M, Friguet B *et al.* How best to halt and/or revert UV-induced skin ageing: strategies, facts and fiction. Exp Dermatol 2008: **17**: 228–240.

Journal of Dermatological Science 61 (2011) 7–13

Contents lists available at ScienceDirect

Journal of Dermatological Science

journal homepage: www.elsevier.com/jds

Review article

Epithelial–mesenchymal transition in the skin

Motonobu Nakamura [a,*], Yoshiki Tokura [b]

[a] Department of Dermatology, University of Occupational and Environmental Health, 1-1 Iseigaoka, Yahatanishi-ku, Kitakyushu 807-8555, Japan
[b] Department of Dermatology, Hamamatsu University School of Medicine, 1-20-1 Handayama, Higashi-ku, Hamamatsu 431-1192, Japan

ARTICLE INFO

Article history:
Received 5 October 2010
Received in revised form 24 November 2010
Accepted 25 November 2010

Keywords:
Epithelial–mesenchymal transition
Snail
SNAI1
Fibrosis
Wound healing
Systemic sclerosis

ABSTRACT

Epithelial–mesenchymal transition (EMT) plays important roles not only in the morphogenesis but also in wound repair, tissue fibrosis and cancer progression. Recently, regulatory mechanism of this process has been elaborately elucidated. EMT can be a new therapeutic target for treating skin ulcer, fibrosing alopecia, and malignant cutaneous cancers, including squamous cell carcinoma and melanoma.

Contents

1. Introduction

Epithelial–mesenchymal transition (EMT) is an intricate process by which epithelial cells lose their epithelial characteristics and acquire a mesenchymal-like phenotype. This dramatic phenotypic change involves the loss of E-cadherin (CDH1)-mediated cell–cell adhesion and prototypic epithelial marker expression, as well as the loss of apical–basal polarity and the acquisition of a motile behavior and a profound reorganization of the cytoskeleton (Fig. 1). Downregulation of CDH1 is one of the essential hallmarks for EMT. As CDH1 plays a crucial role in epithelial homeostasis, its downregulation can lead to decreased expression and/or organization of additional epithelial markers, desmosomal proteins (plakoglobin, desmogleins and desmoplakins), tight junction proteins and cell polarity proteins. Concomitantly, increased expression of mesenchymal markers (e.g., vimentin and fibronectin) as well as extracellular matrix remodeling enzymes (i.e., matrix metalloproteinases) is observed together with profound actin cytoskeleton reorganization. Thus, complex molecular and cellular mechanisms underlie EMT [1,2].

EMT was initially described in early embryogenesis which requires a migration and transient dedifferentiation of embryonic epithelial cells, gastrulation and the migration of neural crest cells. EMT and its reverse process (mesenchymal–epithelial transition,

* Corresponding author. Tel.: +81 93 691 7445; fax: +81 93 691 0907.
E-mail address: motonaka@med.uoeh-u.ac.jp (M. Nakamura).

0923-1811/$36.00
doi:10.1016/j.jdermsci.2010.11.015